



中山大學中法核工程与技术学院

FINAL YEAR INTERNSHIP REPORT

RAPPORT DE STAGE DE FIN D'ETUDES

Family name : CHEN
Given name : Danying
French name : Maeva
Student n° : 14213757

Growth of aluminum nitride on sapphire (0001) by high temperature hydride vapor phase epitaxy and structural characterizations: a design of experiment approach

Year 2015-2016

Defended on (date) 01/06/2016

Name of the hosting institution: Science et Ingénierie des Matériaux et Procédés
Internship time period: 30/11/2015 - 13/05/2016

Hosting institution supervisor: Raphaël BOICHOT
Academic supervisor: Xing Lili

Acknowledgements

I would like to express my deepest gratitude to my supervisor Dr. Raphaël Boichot, for giving me the opportunity to work in the laboratory SIMaP for my final year internship. He encouraged me from the very first, till the last moments of this internship, showing my way to become more professional in scientific research. I would like to thank him for being patient and supportive, in order to correct and help me complete the present dissertation.

I should also thank Dr. Frédéric Mercier who teaches me a lot not in experiments and characterizations, but also in theories. I will always remember the discussions with him, early in the morning in the experimental room, accompanied with our lovely HVPE reactor. Words are not enough to describe his support in all situations (from common everyday issues, up to the preparation for oral talks and analyzing results), helpful scientific discussions and advices. I will carry with me all of their advices, mentality and experience as a priceless gift that was given to me.

I would like also to thank, all members of the CVD team in the group TOP, Nikolaos Tsavdaris, Gaël Giusti, Mikhail Chubarov, and Michel Pons for all their help, support, advices, moments that we share in the experimental room and out of the laboratory. I should give some special thanks to the PhD student Zhang Shiqi doing his experiments with our CVD reactor. Beside his help in analyzing results, he is a very good friend. I would like to thank him for sharing all the moments of anxiety and happiness.

I should thank my institute, Sino-Frenche Institute of Nuclear Engineering and Technology (IFCEN), that gave me the opportunity to accept french-style education and thus led me able to do internship in France. I gained valuable experience for the future and managed to create strong friendships. Also, I should give my acknowledgement to Dr. Xing Lili, for her great help correcting my Chinese report, and sharing her knowledge and experience with me.

Without my boyfriend, I wouldn't be able to complete my internship work. He always encouraged me with patience during all this period. Last, I would like to thank my parents, for all of their support in all of my life.

Attestation sur l'honneur du caractère original du de master

J'atteste par la présente que l'ensemble des résultats présentés dans ce travail ont été réalisés sous la direction de mon superviseur. Mis à part les contenus et les informations dûment référencés, ce mémoire ne comprend pas d'informations produites ou déjà publiées par d'autres individus. L'ensemble des individus et des organisations ayant contribué à la réalisation de ce mémoire sont clairement indiqués. J'atteste avoir pris connaissance des conséquences légales que suppose cette attestation.

Date :

Signature de l'auteur du mémoire :

Droit d'utilisation du mémoire de master

Je soussigné _____ 陈丹莹 _____, déclare avoir pris connaissance des règles de l'université Sun Yat-sen relatives à la conservation et la reproduction des mémoires de master, à savoir : l'université dispose du droit de conserver le mémoire et de le transmettre à des organismes gouvernementaux nationaux sous format électronique et papier, d'émettre une copie partielle du mémoire à des fins non commerciales et de le référencer dans le système d'information de la bibliothèque universitaire, de rendre disponible l'accès au mémoire via la base de données de l'université, de référencer ce travail dans des bases de données nationales ; de reproduire des exemplaires du mémoire, de le scanner ou de l'archiver par d'autres méthodes ; de mettre le mémoire à disposition des bibliothèques universitaires des écoles partenaires de l'université Sun Yat-sen dans le cadre de prêts entre bibliothèques.

Une fois le délai de confidentialité écoulé, de faire valoir la présente attestation.

Date :

Signatures de l'auteur et du superviseur :



中山大學中法核工程与技术学院

FINAL YEAR INTERNSHIP REPORT

RAPPORT DE STAGE DE FIN D'ETUDES

Family name : CHEN
Given name : Danying
French name : Maeva
Student n° : 14213757

Abstract

As one of III-nitride materials, aluminum nitride (AlN) is direct and wide band gap semiconductor, possessing good chemical and thermal stability, and excellent electrical properties. Currently, AlN is proposed as a promising material for many future applications in the domain of energy such as optoelectronics and microelectronics. It also shows technical potentialities in nuclear industry. Despite these interesting potential applications, available process for industrially producing heteroepitaxial AlN layers with freestanding crystal quality is still lacking, which limits the development of AlN-based devices.

This thesis concerns the influence of growth conditions on crystal quality of AlN layers grown on sapphire substrates by high temperature hydride vapor phase epitaxy, and aims to correlate deposition parameters to the crystal defects. Based on the design of experiment method, through a simple linear model without interactions and the Hadamard matrix H16, fifteen parameters are selected for studying their effects. Aspects relative to crystal quality of obtained AlN samples, which contain heteroepitaxial layer thickness, surface roughness, residual stress, density of screw dislocations, are measured by the characterization methods including scanning electron microscopy, atomic force microscopy, Raman spectroscopy, X-ray diffraction, ellipsometry and profilometry. Finally, through the constructed linear model without interactions, main effects of every parameter on each response are analyzed and discussed by a 2σ analysis method. It is observed that all chosen parameters could influence the surface roughness of epitaxial grown AlN. Besides, some parameters have no measurable effect on residual stress and heteroepitaxial layer thickness. Moreover, it is found that the density of screw dislocations is strongly variable but the main parameters influencing it are not highlighted by this screening. This result contradicts the statistic theory, which means that the author should reconsider the parameters. Nevertheless, the presence of interaction and nonlinear terms indicates the lack of accuracy of this model, which forces the author to construct a more complicated model and add experiments.

Keywords: aluminum nitride; hydride vapor phase epitaxy; design of experiment; chemical vapor deposition

Contents

Acknowledgements.....	I
Attestation sur l'honneur du caractère original du de master.....	II
Droit d'utilisation du mémoire de master	II
1. Introduction.....	1
1.1 Context and key issues.....	1
1.1.1 Host laboratory.....	1
1.1.2 Host group.....	2
1.1.3 Key issues	3
1.2 Introduction to aluminum nitride.....	6
1.2.1 Crystal structure	6
1.2.2 Basic properties.....	8
1.2.3 Main applications.....	9
1.2.4 Objectives	12
2. Literature review	15
3. Methodologies.....	17
3.1 Chemical vapor deposition.....	17
3.2 Design of experiment	19
3.2.1 Components of DOE.....	20
3.2.2 Screening.....	20
3.2.3 Post-treatment	21
3.3 Characterization methodes	23
3.3.1 Scanning electron microscopy	23
3.3.2 Atomic force microscopy.....	23
3.3.3 X-ray diffraction	24
3.3.4 Raman spectroscopy	24
3.3.5 Ellipsometry	25
3.3.6 Profilometry	26
4. Results and discussions.....	29

4.1	Experimental configuration	29
4.2	Experimental procedure.....	32
4.3	Selection of parameters and responses.....	34
4.3.1	Substrates	34
4.3.2	Growth parameters	34
4.3.3	Responses.....	38
4.4	Structural characterizations of AlN samples.....	39
4.4.1	X-ray diffraction	39
4.4.2	Surface morphorlogy.....	41
4.4.3	Raman shift	44
4.4.4	Surface curvature	45
4.4.5	Thickness	46
4.5	Results and discussions with DOE.....	48
4.5.1	Influence of each parameter	48
4.5.2	Accuracy of the linear model without interactions	58
4.5.3	Validation	60
5.	Conclusions and perspectives.....	63
6.	References.....	65
7.	Annex	69
7.1.	20-ω XRD spectrum for each sample	69
7.2.	SEM images for each sample	72

1. Introduction

1.1 Context and key issues

1.1.1 Host laboratory



Figure 1.1. Mark of Laboratory SIMaP

SIMaP is the short name of the Materials and Processes Science and Engineering Laboratory. It is a joint Research Unit (UMR 5266) of CNRS and Grenoble INP within the Grenoble Alpes University. It has over 230 people, including research scientists and research lecturers, engineers, technicians, administrative staff, PhDs and postdoctoral research workers.

All of these physicists, material and fluid mechanics specialists and chemists study the preparation, forming, assembly and properties of materials for structural and functional applications (energy, microelectronics, etc.). They combine experimentation and modelling from atomic level to full process scale, based on experimental preparation and characterization facilities.

All staff takes an active part in developing the uses of materials, as a result of which specifications are becoming increasingly complex. There are many possibilities for functionalization: at the surface (surface treatment processes), in the bulk or through assembly (multi-materials). There are still numerous hurdles to be overcome in understanding the phenomena that govern fabrication processes and in modelling and simulating these processes as well as parallel macro-, meso-, and microscopic phenomena in order to anticipate some of the problems that are liable to occur during industrial production.

The main research fields of SIMaP are described as follow:

- The laboratory specializes in particular in the field of metallurgy: phase and interface

thermodynamics, physical chemistry, physical metallurgy, mechanics (forming, behavior and durability), preparation processes (solidification, sintering), control of liquid state (chemistry, fluid mechanics, transfers, wetting);

- It also covers a wide range of topics in the field of ceramics in the broadest sense (sintered ceramics, glasses, monocrystalline oxides).

1.1.2 Host group

In fact, SIMaP is divided into five research groups, sustaining the research on basic sciences of physics and physical chemistry, thermodynamics and kinetics, mechanics of solids and fluids:

- GPM2: Materials and Mechanical Engineering
- PM: Physics of Metals
- TOP: Thermodynamics, Modeling, Process Optimization
- SIR: Surfaces, Interfaces and Reactivity
- EPM: Electromagnetic Processing of Materials

These five groups all participate in the ‘six transversal thematic actions’ to enhance the multidisciplinary skills to spread and share scientific and technical information, and thus to improve the comprehensive strength of the laboratory. The ‘six transversal thematic actions’ are:

- Structural materials
- Nanomaterial – Microelectronics
- Multi-materials and sintering
- Materials for energy
- Solidification and solid-liquid processes
- Multi-scale modeling and simulation

Among these five groups, the group TOP is specializing in high temperature crystal growth of ceramics of the III-IV-V and transition metals groups of elements (SiC, AlN, BN, NbN, TiN) by CVD (Chemical Vapor Deposition).

Actually, this internship project is part of the project EPICEA (Croissance Epitaxiale de Couches Epaisses de Nitre d'Aluminum sur forêt de Piliers). SIMaP is the main and only partner of the project. In fact, the group TOP is involved since 2007 in the growth of epitaxial AlN on various substrates, due to a joint venture with ACERDE Company. During the studies, it has developed various numerical modeling of the HVPE process (mass transport, kinetic and thermodynamic) in parallel to the optimization of the process of epitaxy.

1.1.3 Key issues

Wide band gap III-nitrides have been extensively studied especially in the latest stages of the 20th century. In fact, the initial research work focused on indium nitride (InN), and was gradually oriented towards gallium nitride (GaN), aluminum nitride (AlN) and then bore nitride (BN)^[1].

The historical development of III-nitrides can be divided into three phases. The first phase concerns the synthesis of III-nitrides. The first AlN, GaN and InN were synthesized in 1907, 1910 and 1932 respectively^[2]. However, no significantly useful fabricating process were reported until the end of the 1960s, which shows the fact that III-nitrides had been very difficult to synthesize with good crystal quality at that time.

During 1960s to 1970s (the second phase), it was possible to grow single crystal AlN and GaN thin films due to the development of modern epitaxial growth techniques. The first GaN thin film was successfully elaborated on sapphire substrates in the late 1960s using chemical vapor deposition while the first epitaxial growth of AlN was reported in 1975^[2]. Despite these progresses, it was still hard to produce bulk III-nitrides crystals in this stage.

Since 1980s, researches have focused on the properties and possible applications of III-nitrides. Up to date, the III-nitrides and their ternary alloys based research has attracted considerable attention and gained a significant position in the science and industry of semiconductors due to their wide range of potential applications in optoelectronics and microelectronics^[2].

Optoelectronics is a branch of electronics and photonics that deals with converting

electrical energy to light by solid state semiconductors. Since 1960s, the optoelectronic devices such as optical data storage (DVD, blue-ray and infrared captor), blue/green light-emitting diodes (LEDs), and laser diodes (LDs), have progressively entered people's daily life, and now become essential to the society^[3-5].

The commercialization of candela class GaN-based blue LEDs succeeded in 1993 and two years after the first GaN-based LED under pulse operation was realized^[2,6]. Actually, the high efficiency and high brightness blue LEDs has been demonstrated since a series of fundamental breakthroughs in the area of GaN materials. To date, GaN and its ternary alloy $\text{In}_x\text{Ga}_{1-x}\text{N}$ have been developed for producing short-wavelength LEDs that emit green or blue light^[7,8]. Moreover, AlGaN, the ternary alloy of AlN and GaN, is proposed as an effective material for ultraviolet LEDs (UV-LEDs). This type of LEDs with emission wavelengths in the range of 230 - 530 nm are expected to be used in applications such as water purification, surface disinfection, UV curing, and medical phototherapy^[7].

In microelectronics, III-nitrides also present attractive properties for microelectronic devices. Currently, the GaN/AlGaN system is considered to be the most promising material for High Electron Mobility Transistors (HEMTs). It has been demonstrated that modulation-doped AlGaN/GaN structures have high electron mobility and saturation velocities^[8]. Thanks to these attractive properties, AlGaN based HEMTs offer excellent performance like high power density and high efficiency and enable much high operation voltages as compared to those silicon (Si), gallium arsenide (GaAs), or indium phosphide (InP) based counterparts^[1].

However, many substantial problems should be overcome such as high density of dislocations due to the lack of lattice-matched substrates and also the lack of available process for industrial production before these III-nitrides constitute useful optoelectronic and microelectronic devices.

This report concerns one of the III-nitrides, AlN, and bring some new insight into the field of growth of AlN by high temperature hydride vapor phase epitaxy (HT-HVPE). The aim of the project is to assess the influence of deposition conditions on crystal quality of grown AlN layers and thus to optimize the deposition process. The structure of this report is as following.

In chapter 1, an introduction to its basic properties and main applications is given while the principle idea of this project is mentioned.

In the Chapter 2, a literature review concerning the recent research in China and abroad is shown while in Chapter 3, the growth technique used in our work, a design of experiment method and the characterization method are also presented.

Chapter 4 presents the details of growth process. The experimental configuration that was used is displayed as well as selection of growth parameters. The results of different characterizations including scanning electron microscopy (SEM), atomic force microscopy (AFM), X-ray diffraction (XRD), Raman spectroscopy, ellipsometry, and profilometry are discussed. As a final objective, the influences of each growth parameters are highlighted.

Finally, conclusions and propositions for future studies are given at the end of this report.

1.2 Introduction to aluminum nitride

This section is an introduction to aluminum nitride (AlN). Firstly, a brief overview of its crystal structure, physicochemical properties and main applications is given. In the following part, the objectives of this project are presented.

1.2.1 Crystal structure

AlN is a III-V binary compound semiconductor, combining a cation Al and an anion N. Most of the group III-V binary compounds crystallize in either cubic zinc-blende (ZB) or hexagonal wurtzite (WZ) structure. AlN is trimorphous with wurtzite (B4), zinc-blende (B3) and rock-salt (B1) structures shown in Figure 2.1 with B1, B3 and B4 the Strukturbericht designation for these three phases. At ambient conditions, the stable bulk AlN crystallize in the wurtzite structure.

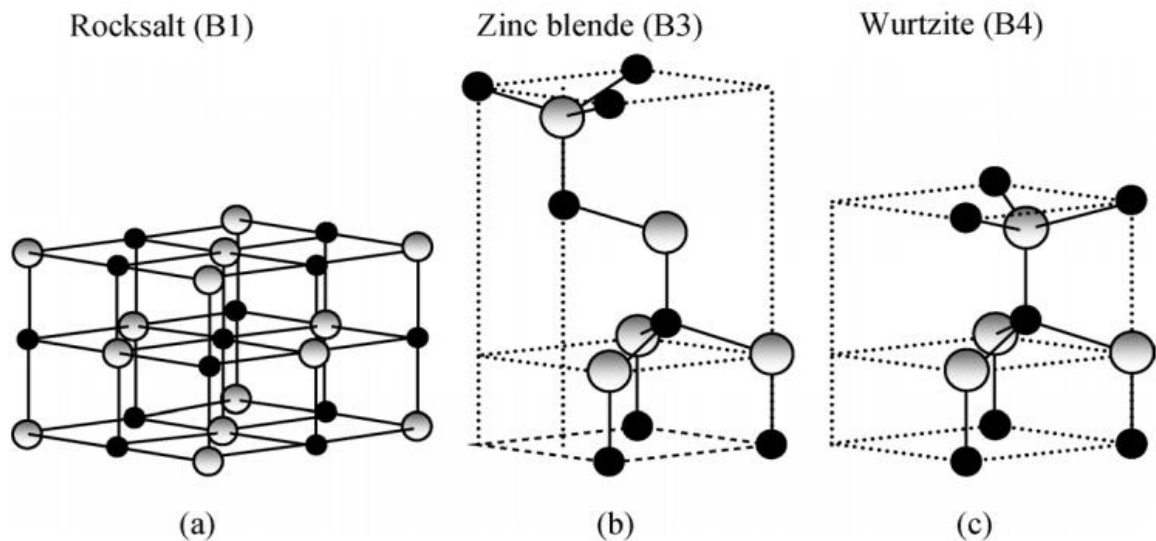


Figure 2.1. Stick-and-ball representation of AlN crystal structures: (a) cubic rocksalt (B1); (b) cubic zinc-blende (B3) and (c) hexagonal wurtzite (B4). Gray and black spheres denote Al and N atoms respectively.

The zinc-blende AlN structure is a metastable phase with the enthalpy very close to that of wurtzite symmetry. It is found that this structure could be stabilized only with a very thin layer and it will transform into the wurtzite structure at larger thickness. And the cubic rock-salt (NaCl) structure may appear under extreme high pressure-high temperature conditions, as in the case of gallium nitride (GaN)^[7].

The hexagonal wurtzite structure belongs to the space group C_{6v}^4 in Schoenflies notation and P6₃mc in Hermann-Mauguin notation. It has two lattice constants c (unit cell height) and a (edge length of the basal plane hexagon) with a ratio of $c/a = \sqrt{8/3} = 1.633$ (in an ideal wurtzite structure). This structure is composed of two interpenetrating hexagonal close packed (hcp) sublattices and each of which is shifted relative to each other along the [001] direction, the so-called threefold c-axis, by the amount of $5/8c$ ^[7-12]. A schematic representation is presented in Figure 2.2.

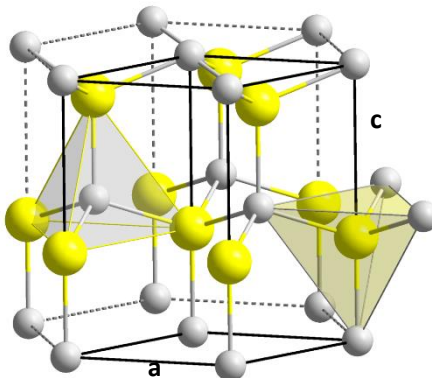


Figure 2.2. Schematic representation of a wurtzitic AlN structure with lattice constants a in the basal plane and c in the basal direction; yellow and gray spheres denote Al and N respectively.

The space group of the metastable zinc-blende phase is denoted by T_d^2 in Schoenflies notation and F $\bar{4}$ 3m in Hermann-Mauguin notation. As shown in Figure 2.3, this structure is considered as two interpenetrating face-centered cubic (fcc) sublattices displaced with respect to each other by one quarter of the body diagonal along the [111] direction^[7-12].

In both structures, each of the Al (N) atoms in the structure is surrounded by four nearest-neighbor N (Al) atoms at the center of a tetrahedron which presents a sp^3 hybridization^[7].

Since the wurtzite structure is the thermodynamically stable phases of AlN at ambient conditions and its crystal quality is higher than that of zinc-blende structure, more and more investigations are carried out for this structure of AlN in recent years. The lattice parameters of wurtzite AlN at room temperature are shown in Table 2.1.

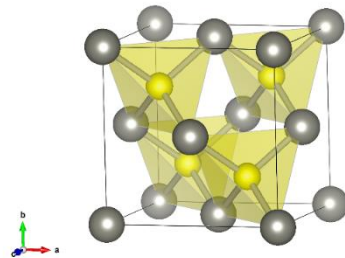


Figure 2.3. Schematic representation of a zinc-blende structure of AlN with lattice constants a in the basal plane and c in the basal direction; gray and yellow spheres denote Al and N respectively.

Table 2.1. Lattice constants of a hexagonal wurtzitic AlN^[7]

Crystal structure	Space group	Lattice constants
wurtzite	P6 ₃ mc	$a = 3.1244 \text{ \AA}$ $c = 4.996 \text{ \AA}$ $\gamma = 120^\circ$

1.2.2 Basic properties

As a III-nitride material, the hexagonal wurtzite AlN is a semiconductor with many interesting intrinsic physicochemical properties such as wide indirect band gap (6.2 eV, 200nm), high thermal conductivity ($3.3 \text{ W}\cdot\text{K}^{-1}\cdot\text{cm}^{-1}$ at 300K), high electrical resistivity ($10^{13} \Omega\cdot\text{cm}$, good mechanical hardness (17.7 GPa at ambient temperature) and low expansion coefficient ($\alpha_a =$

$4.2 \times 10^{-6} \text{ K}^{-1}$ and $\alpha_c = 5.3 \times 10^{-6} \text{ K}^{-1}$). This material is stable to extreme temperatures in inert atmospheres. Moreover, AlN is a piezoelectric material possessing high velocity of surface acoustic wave. Table 2.2 summarized the basic engineering properties of AlN.

Table 2.2. Basic properties of AlN^[7,8,13-17]

Properties		Remarks
Density	3.26 g/cm ³	
Melting point	$\approx 3200 \text{ }^{\circ}\text{C}$	under high pressure conditions
Thermal conductivity	3.3 W·K ⁻¹ ·cm ⁻¹	at 300 K
Thermal expansion coefficient	$\alpha_a = \Delta a/a_0 = 4.2 \times 10^{-6} \text{ K}^{-1}$ $\alpha_c = \Delta a/a_0 = 5.3 \times 10^{-6} \text{ K}^{-1}$	T ranges from 20 to 800 °C a ₀ and c ₀ at 300K
Specific Heat	740 J·kg ⁻¹ ·K ⁻¹	
Mechanical hardness	17.7 GPa	at 300K
Young's module	308 Gpa	
Poisson's ratio	0.24	
Gap energy	Direct gap: 6.2 Ev	at 300 K
Electrical resistivity	$10^{13} \Omega\cdot\text{cm}$	at 300 K
Electrons mobility	300 cm·V ⁻¹ ·s ⁻¹	at 300 K
Holes mobility	14 cm·V ⁻¹ ·s ⁻¹	at 300 K
Breakdown field	$1.2 - 1.8 \times 10^{-6} \text{ V}\cdot\text{cm}^{-1}$	at 300 K
Dielectric constant ϵ	8-9.5	at 300 K

1.2.3 Main applications

Due to its interesting intrinsic properties, actually, AlN has been proposed as a promising material for many future applications in the domain of energy such as optoelectronics and microelectronics. It is also a very good piezoelectric material for surface acoustic wave sensors.

In optoelectronics, AlN serves as buffer layer for AlGaN-based deep UV-LEDs^[7,8,18]. In fact, deep-UV light with wavelength ranging from 200 to 300 nm, is the shortest wavelength that can be used in our environment since the light with wavelength shorter than 200 nm is absorbed by air^[19]. Currently, the available wavelength for UV-LEDs varies from 247 nm to 365 nm^[7]. However, in 2006, a UV-LEV that emits lights with wavelength of 210 nm was successfully produced^[20]. The UV-LEDs are used to purify water or air by photocatalytic reactions. The UV radiation can decompose toxic chemicals and chloride biphenyls by photolysis, and destroy pathogenic bacteria as well. In consequence, the UV-LEDs can be also applied in the field of medical and biology^[7,8,18].

In addition, AlN is also proposed as substrate for the growth of GaN, $\text{In}_x\text{Ga}_{1-x}\text{N}$, and Ga-rich $\text{Al}_x\text{Ga}_{1-x}\text{N}$ used for the fabrication of blue LEDs and blue LDs^[7]. Due to the fact that red and green LEDs have been created and accompanied with human beings for almost half a century and the lack of blue LEDs before 1980s, the revolution of blue brightness LEDs complements the RGB color model in LED technology^[21].

On the other hand, AlN is a suitable substrate for HEMTs^[7]. As mentioned before (see Chapter 1.3), the GaN/AlGaN system presents many attractive properties and offers remarkable potentialities in microelectronics^[7,8,22,23].

Moreover, AlN is among the most promising material for protective coating in extreme conditions. This material can be used as coating for gas turbine in aggressive atmospheres with success. In nuclear industry, polycrystalline AlN coating is proposed as a possible candidate for diffusion barrier to prevent the nuclear fuel-cladding interaction and inter-diffusion under elevated temperatures which is a long term problem that significantly reduce the lifetime of cladding tube.

In fact, the recent development of nuclear fuel cladding technology has promoted the progress of advanced nuclear reactors, including molten salt, fast burner, supercritical water and high temperature reactors. Current promising fuel cladding materials for many of these reactors are ferritic and martensitic stainless steels that isolate the fuel from the coolant^[24,25]. However, the fuel-cladding chemical interaction behavior that occurs at high temperature, due to the fission gas (e.g. lanthanide fission products)-induced fuel swelling and the corresponding contact with the cladding material under irradiation, may cause poorer mechanical properties,

and thus the deformation of the cladding; should be considered in analysis of off-normal fuel operation as well^[27-29].

In order to solve this long term problem, functional coatings on the fuel or cladding that serve as diffusion barrier to prevent inter-diffusion between nuclear fuel and cladding tubes are proposed as an effective method^[24,25]. It is investigated that this type of coatings requires high thermal conductivity, good tolerance to high radiation doses and extreme temperature, and also good resist interaction with both cladding materials and nuclear fuel. Actually, titanium nitride (TiN), a III-nitride material, has been successfully demonstrated the effective diffusion barrier properties between pure iron (Fe) and cerium (Ce) up to 600 °C, and on Ce/TiN/HT-9 (12Cr-1MoVW, one current stainless steel material for nuclear fuel cladding) system at high temperature^[24]. Therefore, the reliability to against the diffusion of Ce and possibly other lanthanide fission products has been proven. Besides, it has been found that the TiN-coated HT-9 material possess excellent hardness and adhesion properties by a thermal cycle test^[24]. Due to its similar physicochemical properties including high thermal conductivity, good oxidation resistance and its excellent diffusion properties, Ickcham Kim et al.^[24] suggested AlN as a promising diffusion barrier to Ce by analogy.

Finally, bulk single crystal AlN is shown to be an excellent candidate for ultrasonic transducers used in harsh radiation environments for non-destructive evaluation (NDE)^[30]. For nuclear power plants, non-destructive evaluation methodology allows complete testing of critical parts without damaging the reactor, which shows highly effectivity and safety. In addition, ultrasound NDE can be used for *in situ* analysis of radiation effects on materials and furthering the understanding of reactor to improve rector safety^[31]. However, the lack of suitable hard piezoelectric material under irradiation for ultrasonic sensors has been considered as an important problem.

To solve this problem, Reinhardt et al.^[30,32] has established selection criteria for piezoelectric materials for NDE and proposed AlN as a viable candidate. It is worth noting that in their studies the wurtzite-structured AlN is considered as a resistant material to amorphization and is predicted to be immune to thermal spike damage in radiation environment^[30]. Their radiation tolerance tests on a bulk single crystal AlN-based ultrasonic transducer have proven the radiation hardness of AlN. It has been also presented that this AlN-based transducer can

operated in a nuclear reactor with success under a fast and thermal neutron flux of 1.85×10^{18} neutrons/cm² and 5.8×10^{18} neutrons/cm² respectively, and a 26.8 MGy gamma dose with no degradation in signal amplitude^[32].

1.2.4 Objectives

Depending on its attractive technical potentialities, various growth techniques have been implemented for synthesizing AlN films, including physical vapor transport (PVT), chemical vapor deposition (CVD), physical vapor deposition (PVD), pulsed laser deposition (PLD), etc. Among these techniques, PVD is the current process used for fabricating AlN BAW and SAW (bulk and surface acoustic waves) piezoelectric devices on silicon substrates. However, this technique leads to poor crystal quality, which would significantly influence the physicochemical properties of AlN layers.

Up to date, the market of AlN single crystals is occupied by PVT crystals. Actually, the PVT method allows to fabricate transparent AlN single crystals with very few visible defects at high temperature and high growth rate. This method has been in development for more than 10 years but it still faces commercial challenges^[6,7,33]. In fact, the major problem of commercial PVT crystals is the oxygen contamination which can greatly affect the thermal conductivity and the electrical and optical properties of AlN, and thus is detrimental to UV transparency for LEDs^[7].

CVD is another promising technique for produce freestanding AlN wafers with industrial grade. This vapor phase growth method includes various variation for growth of AlN, namely, molecular beam epitaxy (MBE), metal organic vapor phase epitaxy (MOVPE, also known as MOCVD and OMVPE) and hydride vapor phase epitaxy (HVPE)^[7,8,34]. MOCVD is currently available to fabricate commercial AlN templates grown at low temperature and low growth rate by using trimethylaluminum (TMAI) and ammonia as precursors for Al and N respectively. However, the pre-reaction between these two precursors usually leads to the incorporation of impurities and polycrystalline growth^[8,35,36]. Nevertheless, the MOCVD process relies on expensive reactors and nevertheless, it suffers from high toxic and pyrophoric nature of

reactants (such as TMAl). These obstacles should have to be overcome to make MOCVD growth of AlN a commercially viable process.

HVPE has been widely considered as an alternative growth technique that offers the advantage of being able to industrially produce AlN with less cost than that of MOCVD and MBE growth. Generally, in this process, the precursor for Al, aluminum chloride, is prepared by the reaction between metal aluminum and chloride gas in furnace, and then reacts with ammonia to deposit AlN layers on the surface of substrate. Since the HVPE process does not require the use of metal-organic precursors which causes unintentional incorporation of impurities (e.g. oxygen and carbon), and the Al-N-Cl-H system is non carcinogenic and non-pyrophoric, it is now proposed as an available technique for industrial production of high crystal purity and high growth rate AlN wafers^[6-8,35,36]. However, despite the commercial success of growth of other III-nitrides, the fabrication of high crystal quality AlN by HVPE is still proven difficult due to high dislocation density of grown layers^[6].

In consequence, the availability of an industrial process for producing thick AlN layers with freestanding crystal quality is still lacking.

On the other hand, AlN is commonly grown on a various of substrates, including but not limited to sapphire, silicon, silicon carbide and PVT AlN. Since the fact that commercial PVT AlN substrates are expensive (more than 1000 euros for a 2 inches' c-plane AlN crystal), the elaboration of AlN is usually done by heteroepitaxial growth^[8]. Sapphire (α -alumina) is among the most promising substrate for heteroepitaxial growth of AlN because of the following advantages:

1. Mature technology for fabrication, very low price, favorable for large-scale manufacturing;
2. Good stability at high temperature;
3. Excellent electrical insulation properties;
4. Transparent broad optical spectrum, which helps to reduce optical absorption for applications in optoelectronics.

Therefore, SIMAP aims to grow high quality heteroepitaxial AlN single crystals on sapphire. However, the stress induced in grown layers, seriously affecting the crystal quality of AlN, is always the major concern with heteroepitaxial growth. This stress may originate from

three main sources during the heteroepitaxial growth of AlN as follow:

1. The first problem is the lattice mismatch between epitaxial layer and the substrate. In almost all cases of interest, the epitaxial layer has a relaxed lattice constant that is different from that of the substrate. In fact, the misfit between AlN and sapphire is 13.7% at ambient temperature. The AlN film might be strained so that its lattice parameters in the lateral direction (i.e. within the growth plane) are forced to match the lattice parameters of sapphire^[7,8]. In-plane dislocations are formed at the AlN/sapphire interface to relax the misfit strain. The stress releasing mechanism by creation of in-plane dislocations is generally not sufficient to accommodate crystal lattices. 3D growth will allow the crystal to reach the unstressed state.
2. As the AlN crystals nucleate and grow on the substrate, mosaicity is created by slight disorientations of these crystals (tilt and twist of about 1°). This allows a complete mechanical relaxation of the nuclei. However, the coalescence of adjacent nanometer-size primary AlN islands induces a strong tensile stress. This phenomenon may introduce new out-of-plane threading dislocations by bending the misfit dislocations;
3. The mismatch of the thermal expansion coefficients between the grown layer and the substrate may lead to a compressive stress into AlN layer when cooling down the {AlN + sapphire} system^[37].

Consequently, the principle idea of the project is to assess the influence of deposition process on AlN crystal quality and thus correlate growth conditions to crystal defects. Finally, an optimized process for producing freestanding AlN single crystals will be proposed. This will be conducted by a Design of Experiment (DOE) method which is presented in Chapter 3.2.

2. Literature review

Although the first synthesis of AlN was reported by F. Briegler and A. Geuther in 1862^[38], for more than a hundred years AlN was merely investigated for its chemistry. Due to the development of modern epitaxial growth process such as MOCVD and MBE in 1970s, it is possible to grow AlN on hetero-substrates, which has greatly attracted researchers' attention^[2]. However, at that time, AlN crystals with high quality were difficult to fabricate.

In recent years, potential applications of AlN have been widely investigated. In order to satisfy the requirements of devices, current researches focus on the development of growth process of AlN for producing high quality AlN with excellent properties. In 1986, H. Amano et al.^[39] proposed a two-step growth method for heteroepitaxial growth of GaN by MOCVD through the growth of an AlN buffer layer at low temperature before the deposition of GaN at high temperature to reduce the lattice mismatch between GaN and sapphire. This method is also widely used in the growth of AlN with the principle idea that is nucleation of AlN at low temperature and growth at high temperature. J. Zhang et al.^[40] discussed the influence of nucleation temperature, nucleation time and the ratio of N/Al on the crystal quality elaborated by MOCVD on sapphire substrates in 2007. M. L. Nakarmi et al.^[41] has developed a three-step growth method for growing high crystal quality AlN epitaxial layers on sapphire by MOCVD. Currently, more and more research institutes study the growth conditions of MOCVD process and aim to develop this process to produce high quality AlN on different substrates.

The growth of AlN by HVPE was once limited by the reaction between quartz and AlCl^[42]. However, it was found that using AlCl₃ as precursor of Al could solve this problem. Moreover, thanks to the successful utilization in the heteroepitaxial growth of GaN, nowadays, HVPE process has been strongly concerned due to its relative low cost. The laboratory SIMaP began to study the growth mechanism of AlN on different substrates by HT-HVPE in 2006^[7]. Through a series of researches combining experiments and simulations, R. Boichot et al.^[43-46] analyzed the relationship between different growth conditions and crystal quality of AlN and aim to optimize current HT-HVPE as an alternative process to produce freestanding AlN crystals with industrial grade. Currently, researches are still in progress.

In China, researches on growth of AlN by HVPE started relatively late. Y. K. Xu et al.^[47] firstly reported the utilization of HVPE process for growing AlN on sapphire. So far, relative researches are still not much.

3. Methodologies

This chapter concerns the growth and the characterizations of AlN. The principle process of the Chemical Vapor Deposition (CVD) technique, which is the growth technique used in this work, is described. A Design of Experiments (DOE) method, a way applied to optimize the outputs of the growth process, is presented. At the end, characterization methods are briefly shown.

3.1 Chemical vapor deposition

Chemical Vapor Deposition (CVD) is a chemical method for producing high quality solid materials. This process combines several scientific and engineering disciplines including thermodynamics, plasma physics, kinetics, fluid dynamics and of course chemistry. It is widely used to deposit different material in various forms: monocrystalline, polycrystalline, amorphous and epitaxial. Compared with Physical Vapor Deposition, CVD can deposit certain elements which have very high melting temperatures such as tungsten, tantalum and carbon^[7].

The CVD process corresponds to the reaction of chemical compounds in the vapor phase near or on heated substrates to form a solid deposit. The principal chemical reactions utilized in CVD growth are thermal decomposition (or pyrolysis), reduction, oxidation, disproportionation and formation reaction. These actions can be used individually or conjunctly^[7,34].

Figure 3.1 shows the basic physicochemical mechanism of an overall CVD reaction with several key steps^[34]:

1. Transport of reagents (i.e. precursors) into the reactor;
2. Gas phase reactions of precursors in the reaction zone;
3. Diffusion of the reactants to the substrate surface;
4. Adsorption of reacting species on the substrate surface;

5. Surface diffusion of adsorbed reactants to preferential sites (ledge, defects...) and formation of constituent crystallite of the solid film;
6. Desorption and mass transport of reaction products away from the reaction zone.

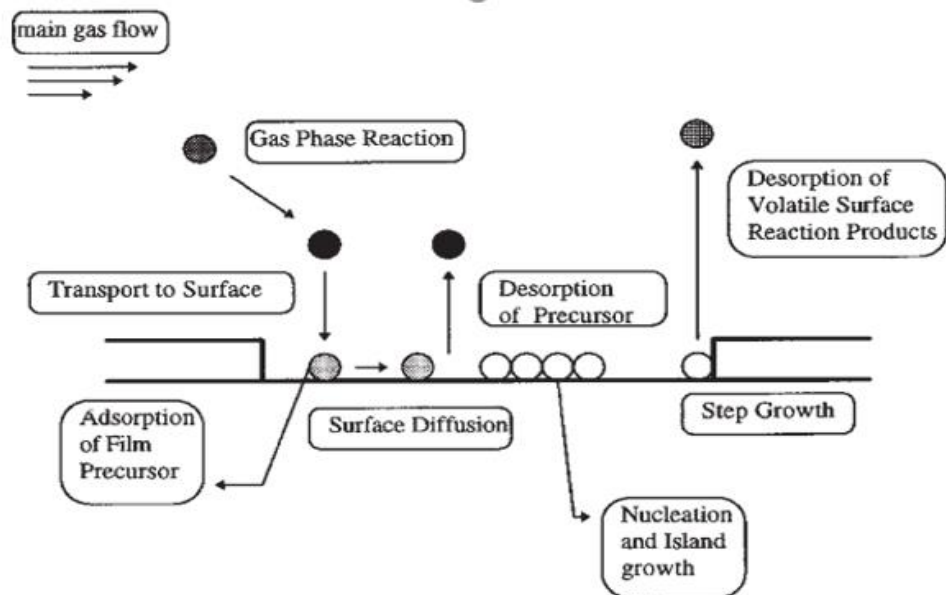


Figure 3.1. Precursor transport and reaction process in CVD^[34]

3.2 Design of experiment

The Design of Experiment (DOE) method is a systematic procedure widely used in scientific research and also in industrial settings. It is involved in many industrial fields including chemical, mechanical, automotive and metallurgical industries. The principal idea of this method is usually to establish the simplest model that can determine the effect of multiple process input factors on desired outputs (responses) and optimize these outputs with the lowest deviation of the model to the experimental data while minimizing the necessary number of experiments since varying one parameter at a time is a waste of time and money^[48]. The DOE is a sequential method promising to construct the other more complex models with defined steps as shown in Figure 3.2:

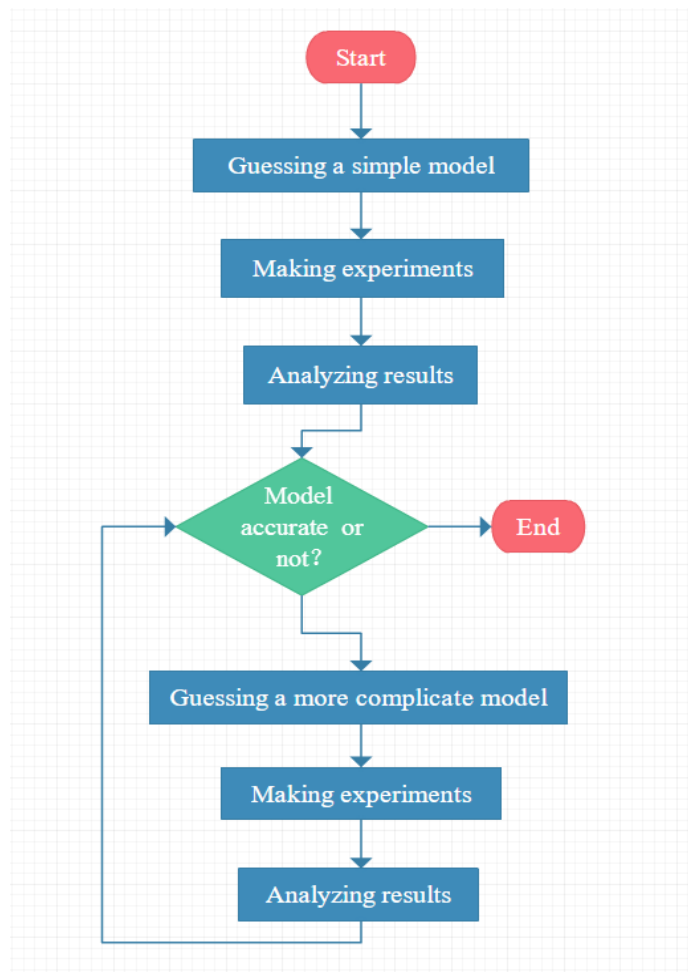


Figure 3.2. Principle steps of a DOE method

3.2.1 Components of DOE

Before the beginning of a DOE, three aspects of the process should be analyzed:

1. Parameters, or process inputs. In fact, parameters can be classified as either controllable or uncontrollable variables. Typically, the controllable parameters are those inputs that can be modified while the uncontrollable parameters should be fixed in the process. All parameters, even ridiculous, need to be taken into account or at least measured. Classically, the degree of freedom in parameter selection is $2^n - 1$;
2. Levels, or setting of each parameter. Generally, parameters P_i could be coded as orthogonal variables X_i by definition $X_i = \frac{P_i - (P_{imax} + P_{imin})/2}{P_{imax} - P_{imin}} = \frac{P_i - P_{iavg}}{\Delta P_i/2}$. In this case, the non-dimensional variables of continuous parameters would vary in the same range [-1, 1] and the high and low levels of discrete parameters are coded as +1 and -1;
3. Responses, or outputs of the experiment. Experimenters should plan carefully what outputs to be measured and analyzed to avoid optimizing the process for one response at the expense of another (no discrete response allowed).

After the selection of those components above, it is necessary to ensure the experiment process is stable and repeatable. To this purpose, experimenters should choose a ‘central’ working point (choose one level for discrete parameters and middle of the setting range for continuous parameters) and repeat it at least three times. It also needs to be verified that every measured response of these repetitions should have an average value that is twice larger than its standard deviation^[48]. Once the repeatability of responses is verified, the DOE can begin.

3.2.2 Screening

According to the DOE process shown before, the first step is to construct a linear relationship without interactions (the simplest model) between responses and parameters:

$$R_i = A_{i,0} + \sum_{j=1} A_{i,j} P_j \quad (3-1)$$

where R_i is the i^{th} response, $A_{i,j}$ the j^{th} non-dimensional coefficient for response R_i and P_j the j^{th}

non-dimensional parameters that varies in the interval [-1, 1].

To find the optimal statistical properties in the whole experimental domain, Hadamard matrix is used for the determination of non-dimensional coefficients. This matrix is constructed by recurrence:

$$H_1 = [1] \quad H_2 = \begin{bmatrix} 1 & 1 \\ 1 & -1 \end{bmatrix} \quad H_n = \begin{bmatrix} H_{n-1} & H_{n-1} \\ H_{n-1} & -H_{n-1} \end{bmatrix} \quad \text{and} \quad {}^t H_n \cdot H_n = n \quad (3-2)$$

with $n = 2^k$ and k the natural number.

Consequently, the coefficient i of the model for the response k is simply deduced by the following formula:

$$A_{i,k} = \frac{1}{n} \sum_{k=1}^n H_n(j,i) \cdot R(j,k) \quad (3-3)$$

where R is the $n \times m$ dimensional matrix containing the response for each experiment with m the number of responses and n that of coefficients.

Theoretically, it needs only n experiments for n coefficients ($n-1$ parameters). The order of experiments is unspecified. It is convenient to add a ‘-1 experiment’ as the last experiment with each parameter set to -1 for post-treatment.

3.2.3 Post-treatment

Since in the linear model constructed before the coefficients have no dimensions, it is reasonable to compare their absolute value (except the first one, the so-called y -intercept coefficient) directly to two times the standard deviation of repetitions ($2SD$, written in 2σ), to assess the influence of inputs to a given response. While the absolute value of $A_{i,k}$ is larger than 2σ , it means that the parameter P_i has a measurable impact on response R_k , and vice versa.

To confirm that this simple model is accurate at the boundaries, it is necessary to compare the theoretical value calculated by the model to the experimental data of ‘-1 experiment’:

$$R_{\text{theoretical, exp-1}} = A_0 + [-1 \ \dots \ -1]_{1 \times n} \cdot \begin{bmatrix} A_1 \\ \vdots \\ A_n \end{bmatrix}_{n \times 1} \quad (3-4)$$

If $R_{\text{theoretical, exp-1}} - R_{\text{-1 experiment}}$ is larger than 2σ , it can be concluded that this model is accurate at the extrema of the whole experimental domain. Otherwise, linear interaction terms

should be added, which will push the number of experiments to 2^{n-1} for n coefficients (complete factorial design):

$$R = A_0 + \sum_{i=1} A_i P_i + \sum_{i=1, j \neq i} A_{ij} P_i P_j + \sum_{i=1, j \neq i, k \neq i} A_{ijk} P_i P_j P_k + \dots \quad (3-5)$$

It is also necessary to confirm the accuracy of the model at the center. This will be done by comparing the experimental result with the theoretical value of the ‘central’ working point:

$$R_{\text{theoretical, central}} = A_0 + [0 \ \cdots \ 0 \ 1 \ -1 \ \cdots]_{1 \times n} \cdot \begin{bmatrix} A_1 \\ \vdots \\ A_n \end{bmatrix}_{n \times 1} \quad (3-6)$$

If $R_{\text{theoretical}} - R_{\text{central experiment}}$ is larger than 2σ , this linear model without interactions is accurate at the center, and it is therefore suitable for the whole experimental domain. Otherwise, it needs to add nonlinear terms like:

$$R = A_0 + \sum_{i=1} A_i P_i + \sum_{i=1} A_{ii} P_i^2 + \sum_{i=1} A_{iii} P_i^3 + \dots \quad (3-7)$$

Once a model works, it must be assessed with relevant statistical tools: residual analysis, Jarque Bera tests, R^2 analysis, adjusted R^2 analysis and etc.

However, it is worth noting that DOE is not a tool intended a priori to fundamental research since it could not explain physicochemical phenomenon^[48].

3.3 Characterization methods

In this paragraph, the characterization techniques used in this study are summarized.

3.3.1 Scanning electron microscopy

Scanning electron microscopy (SEM) is a method for high-resolution imaging of surfaces. The scanning electron microscope uses electrons instead of light to form an image. Since their development in the early 1950's, scanning electron microscopes have developed new areas of study in the medical and physical science communities, allowing researchers to examine a much bigger variety of specimens.

In fact, the principle idea is that incident electrons interact with the sample, producing various signals that can be used to obtain information about the surface topography and composition.

3.3.2 Atomic force microscopy

The atomic force microscope (AFM) is one kind of scanning probe microscopes (SPM).

To acquire the image resolution, AFMs can generally measure the vertical and lateral deflections of the cantilever by using the optical lever. The optical lever operates by reflecting a laser beam off the cantilever. The reflected laser beam strikes a position-sensitive photo-detector consisting of four-segment photo-detector. The differences between the segments of photo-detector of signals indicate the position of the laser spot on the detector and thus the angular deflections of the cantilever.

3.3.3 X-ray diffraction

X-ray diffraction (XRD) is an important characterization tool to study crystallographic properties of the epitaxial layers. In fact, the wavelength of X-ray and the typical inter-atomic distance in crystalline solids are on the same order (a few angstroms, $1\text{\AA} = 0.1\text{nm}$), which makes X-rays the correct order of magnitude for diffraction of atoms of crystalline materials. XRD can provide structural information such as lattice constants, orientation, strain and dislocation density in the layer.

The experimental set-up of a diffractometer consists of an X-ray source equipped with a monochromator, and a gas ionization detector, and the sample to be analyzed as shown in Figure 3.4. Bragg explains the interference of X-rays from lattice planes by following equation:

$$n\lambda=2d_{hkl}\sin(\theta) \quad (3-8)$$

where λ the wavelength of x-rays, d_{hkl} the lattice plane spacing, n the order of the reflection and 2θ the angle between incident and reflected X-ray.

Two basic types of scans, namely, ω scan and $\omega-2\theta$ scan, are usually used for structural characterizations to provide information about crystal quality of the measured material. ω is the angle between incident X-ray and sample surface whereas 2θ represents the detector angle. In the ω rocking curve measurement, the 2θ is fixed to the position $2\theta_0$ of the Bragg peak. In this case, only one lattice plane spacing will be studied. ω is tilted around the Bragg peak. ω scan is sensitive to strain, dislocations and mosaic structure in thin films.

3.3.4 Raman spectroscopy

Raman spectroscopy is a non-destructive technique to characterize the vibration mode of materials. It relies on inelastic scattering of photons. When a beam of laser light illuminates a sample, a few of the photons will impinge upon the sample molecules and be rebounded. Most of the collisions are elastic, called Rayleigh scattering, which means no transition of energy occurs between the photon and the molecules. However, if there is energy shift between photon and molecule, the scattering is called Raman scattering. Precisely, the phenomenon is called

Stokes scattering or Anti-Stokes scattering respectively when the energy of the photo shifts down or up. The energy shift of the photo or Raman shift is typically reported in wavenumbers, which have units of inverse length, as this value is directly related to energy. The Raman shift can be expressed as the formula below:

$$\Delta\omega(\text{cm}^{-1}) = \left(\frac{1}{\lambda_0(\text{nm})} - \frac{1}{\lambda_1(\text{nm})} \right) \times \frac{(10^7 \text{ nm})}{(\text{cm})} \quad (3-9)$$

where $\Delta\omega$ is the Raman shift expressed in wavenumber, λ_0 the excitation wavelength, and λ_1 the Raman spectrum wavelength.

Moreover, Anastassakis et al. has reported that this technique could be sensitive to study mechanical stress. Particularly, the micro-Raman spectroscopy (μ RS) is used more and more for characterizing local stress in heteroepitaxial layers.

3.3.5 Ellipsometry

Ellipsometry is a very sensitive optical non-destructive technique for the characterization of surfaces and thin film layers. Due to the fact that polarization state of light may change when the light beam is reflected from a surface, it is possible to be used for derive information about the surfaces. In fact, if the surface is coved by a thin film, the entire optical system {film + substrate} will influence the change in polarization. Therefore, it is usually used to determine thin film properties, mainly the film thickness.

A schematic set-up of a nulling imaging ellipsometer is presented as Figure 3.5. In most types of ellipsometers, the main optical components are polarizer which products light in an especial state of polarization at its output and analyzers that is a second polarizer. The unpolarized incident light emitted by a light source is polarized by rotating the polarizer and then pass through an optional compensator. Reflected light passes sequentially another compensator and then the analyzer, and finally falls into the detector.

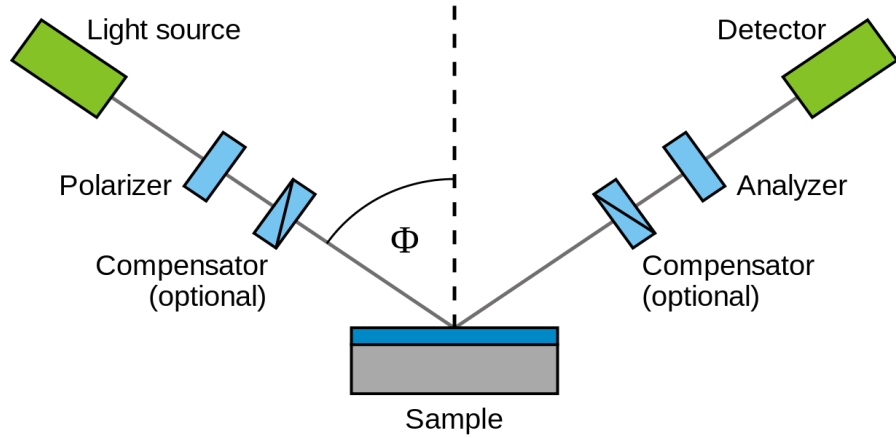


Figure 3.5 Experimental set-up of an ellipsometer

In ellipsometry measurements, the incident angle equals the angle of reflection. A plane called plane of incidence is spanned by the incident and reflected beam. It is common to define the polarization direction that is parallel to this plane as p-polarized and s-polarized for the polarization direction perpendicular. The ellipsometry measurement relies on two parameters, φ and Δ , the ratio of relative amplitude and phase difference for p-polarized and s-polarized light before and after reflecting on sample surface. The ration of complex reflection, denoted by ρ , is in terms of φ and Δ as follow:

$$\rho = \tan(\varphi) e^{i\Delta} \quad (3-10)$$

Since ellipsometry is an indirect method, for analyzing acquired data, it needs the construction of a layer model which contains the optical constants and thickness parameters of all individual layers of the sample. Iterative methods such as Cauchy functions are usually used to determine layer thickness and optical constants.

3.3.6 Profilometry

Profilometry is a common tool to measure the surface characteristics of films. This method is based on the contact measurement of the sample. During the measurement, a stylus is scanned through the sample surface and the vertical displacement of the stylus is converted into a height value in z direction corresponding to the height at each measured point of the sample. With the scan date, the radius of surface curvature can be calculated. However, since this method requires

the direct contact with the sample, it is possible to damage the sample and it is not suitable for in situ measurements.

4. Results and discussions

This chapter is dedicated to the experimental study of the development of deposition process of AlN films. In the first part, the used reactor and operating procedure will be briefly described. Then, the selection of growth parameters and measured responses are summarized, followed by the structural characterizations of AlN films. Discussions about effects of each parameter on crystal quality of AlN are presented. Finally, the accuracy of the constructed linear model is verified through the DOE method.

4.1 Experimental configuration

In our project, the fabrication process of AlN is High Temperature Halide Vapor Phase Epitaxy (HT-HVPE). This process uses aluminum chloride and ammonia (Goodfellow 99.999%) as precursors in hydrogen (99.999%) as carrier gas, and AlN layers are grown on the surface of substrate according to the following reaction:



The experimental setup used is a water-cooled vertical cold-wall quartz reactor working at low pressure which consists of two principal compartments. Schematics of this reactor are shown as Figure 4.1.

The first part is a small quartz tube filled with aluminum pellets (99.999%), the so-called chlorination chamber. A gas inlet is located on the top of this quartz tube while its lower part consists of a piece of sintered quartz allowing evacuation of gas after passing through the aluminum pellets. In fact, during the experiment, this chlorination chamber is heated by a heating lamp for *in situ* synthesis of aluminum chloride AlCl₃ (g) via the reaction between aluminum and chlorine (99.999%). Chlorine is chosen rather than hydrogen chloride to separate the effect of Cl and H and to avoid too corrosive atmosphere in the chlorination chamber.

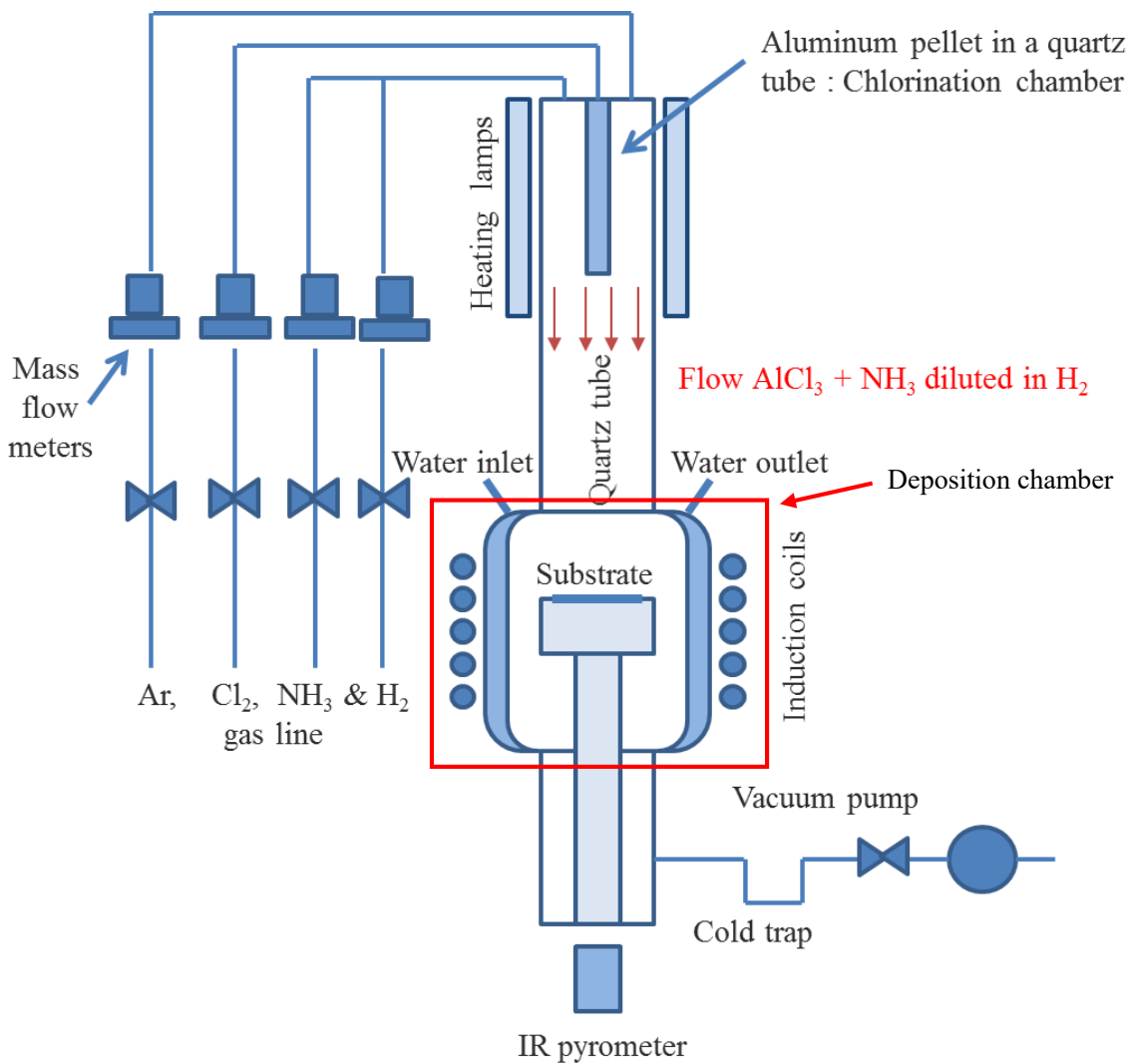


Figure 4.1. Experimental set-up of the used CVD reactor.

The second part is the deposition chamber of the reactor. In this part, the inner wall of the quartz reactor is cooled by circulating recycle water (temperature between 10 and 20 °C depending on the season) to minimize the reaction between traces of aluminum monochloride AlCl (g) and quartz. The throttle of reactor located between these two chambers is maintained above 200 °C using a heating tape to prevent the condensation of precursors on the walls. Substrate is placed on a graphite holder heated by induction. An infrared pyrometer which allows monitoring of the deposition temperature between 700 and 1800 °C is aimed at the edge of the substrate for temperature measurement.

Actually, neutral argon gas with high purity (99.999%), hydrogen and ammonia are introduced into the upper part of reactor without contact with the chlorination chamber. And

then ammonia reacts with synthesis AlCl₃ gas to deposit AlN on the surface of substrate. The gas flow rates are controlled by flow meters.

The whole reactor is pumped by a volumetric pump (oil) that provides primary vacuum inside the reactor. A cold trap cooled with ice/water mixture is used to capture and condense chlorinated gas which could damage the pump during operation. The total pressure is controlled by a butterfly valve while it is measured by a Baratron gauge ranging from 0 to 100 mbar.

4.2 Experimental procedure

The objective of this section is to explain the whole experimental procedure for depositing AlN layers from the preparation to the extraction of the sample.

The chlorination chamber is filled with aluminum pellet and well installed while the substrate is placed on the graphite holder before the close of reactor. The reactor is subsequently evacuated at ambient temperature. Once vacuum is achieved, the CVD experiment can be started.

Firstly, the reactor is purged by argon at least three times. This step aims to evacuate the external impurities (e.g. adsorbed water) in the reactor. In order to purify the aluminum pellet and limit the contamination of oxygen, the chlorination chamber is heated up to about 650 °C and cleaned by hydrogen at a flow rate of 0.2 slm. After that, the graphite is inductively heated under hydrogen with a fixed ramp-up rate of 2%/min (about 20 °C/min). Finally, hydrogen annealing of the sample is undertaken at 1100 °C for substrate cleaning.

The previously description is the common part of all experimental operation. The next phase concerns the growth of AlN layers on sapphire which comprise different modes to be described as follow. In fact, it has been investigated that the pulsed flow method using in the growth of AlN by MOCVD can enhance the migration of aluminum atom on the surface of substrate, which leads to better smoothness of AlN epitaxial layers^[49]. Consequently, three different types of gas injection are employed during the deposition for migration enhancement: chlorine and ammonia are continuously or simultaneously or sequentially introduced into the reactor as shown in Figure 4.2(a), (b) and Fig. (c) respectively. The deposition contains 1000 cycles for the pulsed mode injection while the deposition time for continuous mode is 1000 seconds. The purge gas, hydrogen, is used to transport the reaction products and the non-reactants away from the reaction zone.

After the deposition and cooling down procedure, the reactor is purged by argon for three times to evacuate impurities (e.g. chlorides).

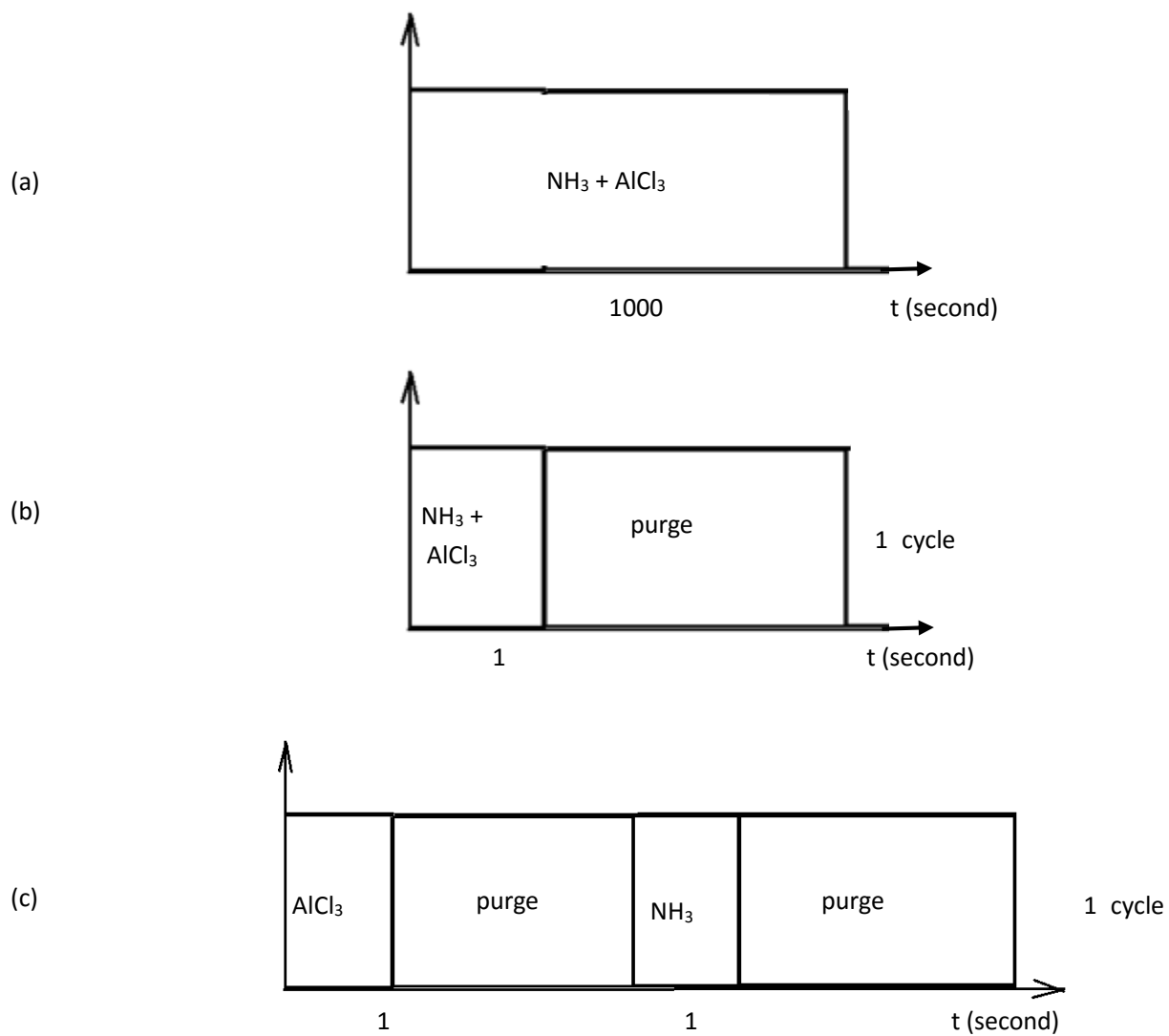
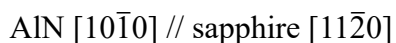
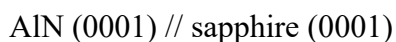


Figure 4.2 Schematic representation of the three different gas injection modes

4.3 Selection of parameters and responses

4.3.1 Substrates

The substrates used in the project are the 2 inches' sapphire (0001) wafers fabricated by the company RODITI. Sapphire (α -Al₂O₃) is being used extensively as a substrate for III-nitrides. It is defined by a rhomboidal lattice (lattice constants of $c = 5.1304 \text{ \AA}$ and $a = 4.758 \text{ \AA}$) and belongs to the space group R3c. For a (0001) oriented sapphire substrate, the relationship for epitaxial growth between hexagonal wurtzite AlN and sapphire is shown as follows:



The lattice mismatch between these two structures is 13.7% at ambient temperature, which will induce a great number of defects in the grown layers.

4.3.2 Growth parameters

In previous section, the experimental procedure is presented with details. Since CVD experiments are expensive and it needs nearly one day for doing an CVD experiment, the DOE method described before (see Chapter 3.2) is employed in order to study the influence of deposition conditions on AlN crystal quality.

Finally, 15 parameters are chosen as variable inputs and 9 factors are fixed. The fixed parameters include: point of temperature measurement for pyrometer (aimed at the edge of the substrate); length of aluminum pellets in chlorination chamber (4 centimeters); size and length of quartz tubes (diameter of 65 mm and length of 1 m); 1000 deposition cycles described as before (1 second for each pulse of active gas); 2 inches' RODITI sapphire (0001) wafers; procedure for cleaning the CVD reactor (hot water + HCl - Distilled water - ethanol - isopropanol), old substrate holder ; Cl₂ = 2sccm; Ramp up rate = 2%/min.

With respect to the principle idea of the DOE method, variable parameters are classified as either discrete or continuous factors. After that, they are transformed by definition into non-dimensional variables that belong to the interval [-1, 1]. 15 parameters are chosen and thus the Hadamard matrix H_{16} is used for designing experiments. All selected deposition parameters are presented in Table. 4.1.

Table 4.1. Growth parameters for depositing AlN

	Parameters	-1	0	+1
1	aluminum pellet age	used once		new
2	cooling down gas	$H_2 + 10 \text{ sccm}$ NH_3		1 slm N_2
3	mounting delay	the day before		during the day
4	aluminum pellet size	small		large
5	gas injection mode	sequential		simultaneous
6	aluminum flow rate	1.33 sccm	2.66 sccm	3.99 sccm
7	purge time	0 second	2 seconds	4 seconds
8	pre-chlorination time	0 second	1 seconds	2 seconds
9	etching time at 1100 °C	0 minutes	10 minutes	20 minutes
10	pellet cleaning under hydrogen	10 minutes	20 minutes	30 minutes
11	hydrogen flow rate	0.5 slm	1 slm	1.5 slm
12	furnace power	40%	45%	50%
13	cooling down rate	1%/min	2%/min	3%/min
14	growth temperature	1200 °C	1250 °C	1300 °C
15	total pressure	10 torrs	15 torrs	20 torrs

In fact, the inductively heating up and cooling down rate are controlled through a high power electric generator. 1% equals nearly 10 °C during the experiments. The pellet cleaning step is used to evacuate impurities and prevent the oxidation of aluminum pellets. The furnace power in the range from 40% to 50% corresponds to the temperature ranging from 600 to 650

°C which is the predominant domain for the synthesis of AlCl₃.

For the ‘central’ repetitions, all variable parameters are set as 0. For the discrete parameters, the ‘safe’ set-point are chosen. ‘Safe’ means that with these set-points, the deposition will be done in a safe-enough environment (e.g. cooling down under non-active gas atmosphere) and the crystal quality of obtained repetition samples are as predicted (respected to previous word done in SIMaP). Therefore, values of discrete parameters for ‘central’ experiments are shown in Table 4.2.

Table 4.2. Set-points of the discrete parameters for ‘central’ repetitions.

Parameter	Value	Relative set point
P1: aluminum pellet age	+1	new
P2: cooling down gas	+1	under 1 slm N ₂
P3: mounting delay	+1	during the day
P4: aluminum pellet size	-1	small
P5: gas injection mode	-1	sequential

In convention, ‘R’ represents the ‘central’ repetition experiments and ‘H’ denotes Hadamard in the following discussions. Finally, deposition processes for each experiment are presented in Figure 4.3.

Pellet age	Cooling down gas	Mounting delay	Pellet size	Injection	NH3	Purge time	Pre-AlCl ₃	Etching time at 1100 degree under hydrogen	H2	Pellet cleaning	Cooling down rate	Temperature (degree)	Pressure (tons)	
R1	new	N2	during the day	small	sequential	2.66sccm	2 seconds	1 min	10 min	20 min	1000sccm	45%	2%/min	1250 15
R2	new	N2	during the day	small	sequential	2.66sccm	2 seconds	1 min	10 min	20 min	1000sccm	45%	2%/min	1250 15
R3	new	N2	during the day	small	sequential	2.66sccm	2 seconds	1 min	10 min	20 min	1000sccm	45%	2%/min	1250 15
H1	new	N2	during the day	large	simultaneous	3.99sccm	4 seconds	2 min	20 min	30 min	1500sccm	50%	3%/min	1300 20
H2	used once	N2	before the day	large	sequential	3.99sccm	no	2 min	no	30 min	500sccm	50%	1%/min	1300 10
H3	new	H2	before the day	large	simultaneous	1.33sccm	no	2 min	20 min	10 min	500sccm	50%	3%/min	1200 10
H4	used once	H2	during the day	large	sequential	1.33sccm	4 seconds	2 min	no	10 min	1500sccm	50%	1%/min	1200 20
H5	new	N2	during the day	small	sequential	1.33sccm	no	2 min	20 min	30 min	1500sccm	40%	1%/min	1200 10
H6	used once	N2	before the day	small	simultaneous	1.33sccm	4 seconds	2 min	no	30 min	500sccm	40%	3%/min	1200 20
H7	new	H2	before the day	small	sequential	3.99sccm	4 seconds	2 min	20 min	10 min	500sccm	40%	1%/min	1300 20
H8	used once	H2	during the day	small	simultaneous	3.99sccm	no	2 min	no	10 min	1500sccm	40%	3%/min	1300 10
H9	new	N2	during the day	large	simultaneous	3.99sccm	4 seconds	no	no	10 min	500sccm	40%	1%/min	1200 10
H10	used once	N2	before the day	large	sequential	3.99sccm	no	no	20 min	10 min	1500sccm	40%	3%/min	1200 20
H11	new	H2	before the day	large	simultaneous	1.33sccm	no	no	no	30 min	1500sccm	40%	1%/min	1300 20
H12	used once	H2	during the day	large	sequential	1.33sccm	4 seconds	no	20 min	30 min	500sccm	40%	3%/min	1300 10
H13	new	N2	during the day	small	sequential	1.33sccm	no	no	no	10 min	500sccm	50%	3%/min	1300 20
H14	used once	N2	before the day	small	simultaneous	1.33sccm	4 seconds	no	20 min	10 min	1500sccm	50%	1%/min	1300 10
H15	new	H2	before the day	small	sequential	3.99sccm	4 seconds	no	no	30 min	1500sccm	50%	3%/min	1200 10
H16	used once	H2	during the day	small	simultaneous	3.99sccm	no	no	20 min	30 min	500sccm	50%	1%/min	1200 20
R4	new	N2	during the day	small	sequential	2.66sccm	2 seconds	1 min	10 min	10 min	1000sccm	45%	2%/min	1250 15
Exp-1	used once	H2	before the day	small	sequential	1.33sccm	no	no	no	10 min	500sccm	40%	1%/min	1200 10

Figure 4.3. Parameters for each experiment

4.3.3 Responses

According to J.E. Ayers^[50], mismatched heteroepitaxial growth contains several important aspects mainly including layer thickness, dislocation and defect densities, strain and stress, as well as surface roughness. These characteristics can be analyzed through the structural characterization methods shown before (Chapter 3.3). Therefore, 6 responses are chosen and presented in the following table:

Table 4.3. Responses for analyzing crystal quality of AlN films

	Response	Characterization methods
1	Layer thickness in nm	Ellipsometry
2	Ra roughness at the center of the sample in nm	AFM
3	RMS roughness at the center of the sample in nm	AFM
4	FWHM rocking curve peak symmetric (0002) in arcsec	XRD
5	Raman shift for E ₂ (high) phonon mode of AlN in cm ⁻¹	Raman spectroscopy
6	Surface curvature in m ⁻¹	Profilometry

4.4 Structural characterizations of AlN samples

According to the chosen responses, the structural characterizations of AlN films grown on sapphire were done by SEM, AFM, XRD, Raman spectroscopy, ellipsometry, and profilometry. The analysis of these characterizations are presented in this section. Finally, all measured responses data are summarized.

4.4.1 X-ray diffraction

The XRD measurements were performed at Cu K α wavelength by using a X'PERT PRO MPD PANalytical X-ray diffractometer. 2 θ - ω scan and on-axis ω rocking curves for (0002) AlN refection were measured for all samples.

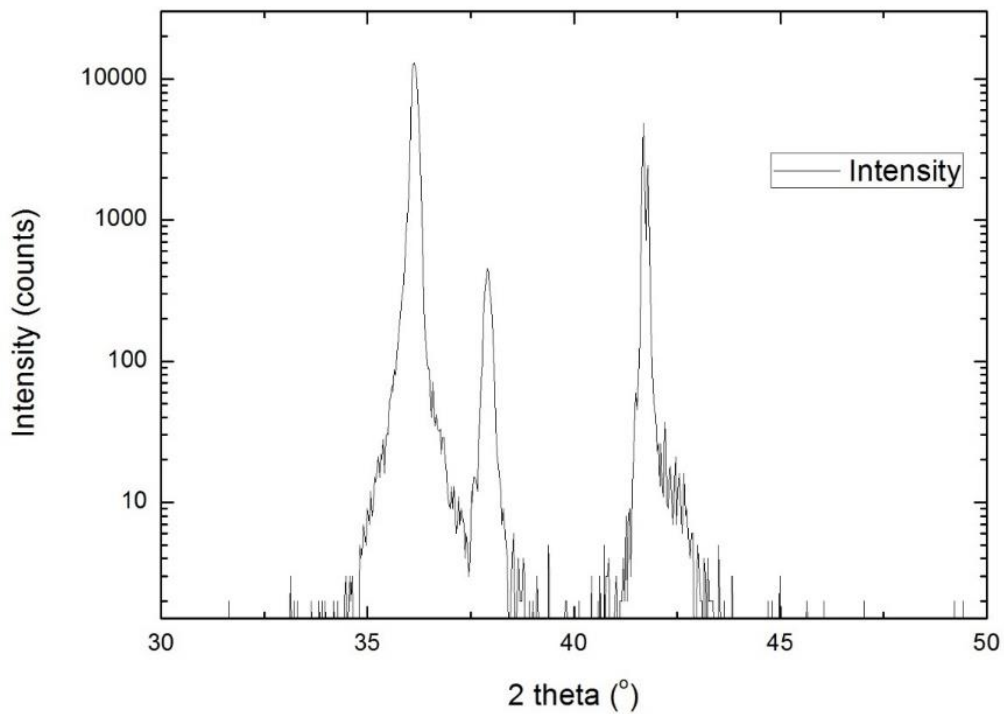


Figure 4.4. XRD 2 θ - ω scan spectrum of the sample AlN-30 with respect to H5

The XRD patterns of our 21 samples fit well with file No. 25-1133 of JCPDS-ICDD diffraction database PDF-2. Figure 4.4 presents the XRD $2\theta-\omega$ scan spectrum of the polycrystalline sample AlN-30 with respect to H5. Spectra of other samples are shown in annexes. The abscissa of the figure is the angle of diffraction 2θ and the ordinate is the intensity of diffracted X-rays. The scan range (2θ) is from 30° to 50° while the diffraction rate is with $\Delta(2\theta) = 0.001^\circ$.

The most intensive peak observed at 36.08° indicates the presence of AlN (002) preferential orientation while the (101) peak locates around 37.90° ; and the moderate intensive peak at 41.80° is correlated to sapphire (006) reflection. Among all obtained samples, the orientation (101) is observed only in five samples, namely, AlN-14, AlN-16, AlN-19, AlN-20, AlN-30, corresponded to H4, H6, H9, H10, H15 respectively.

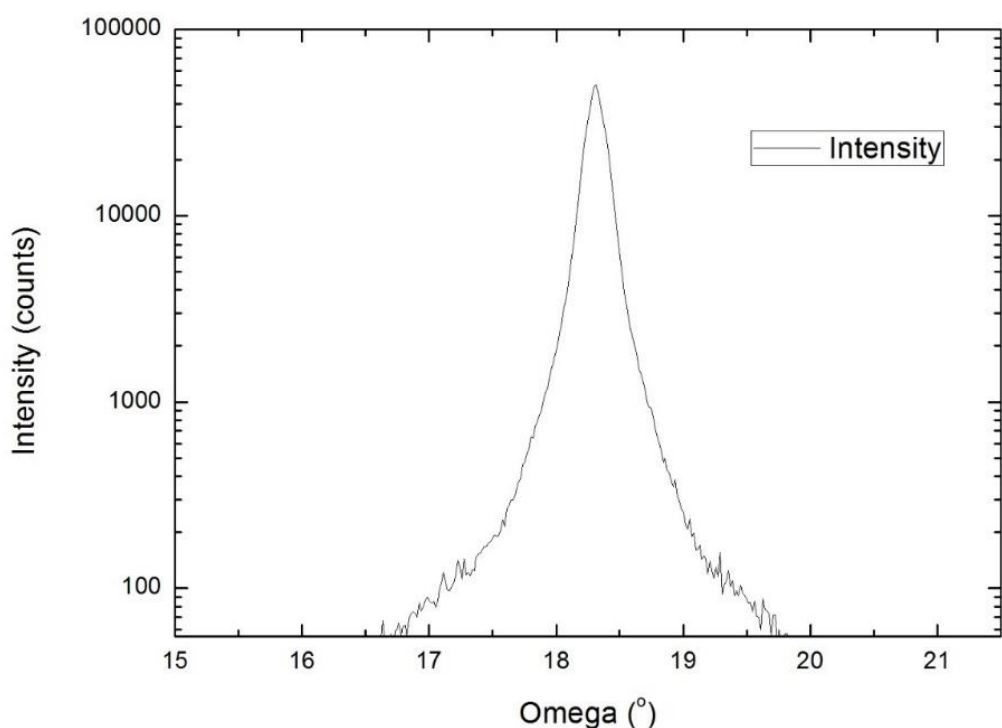


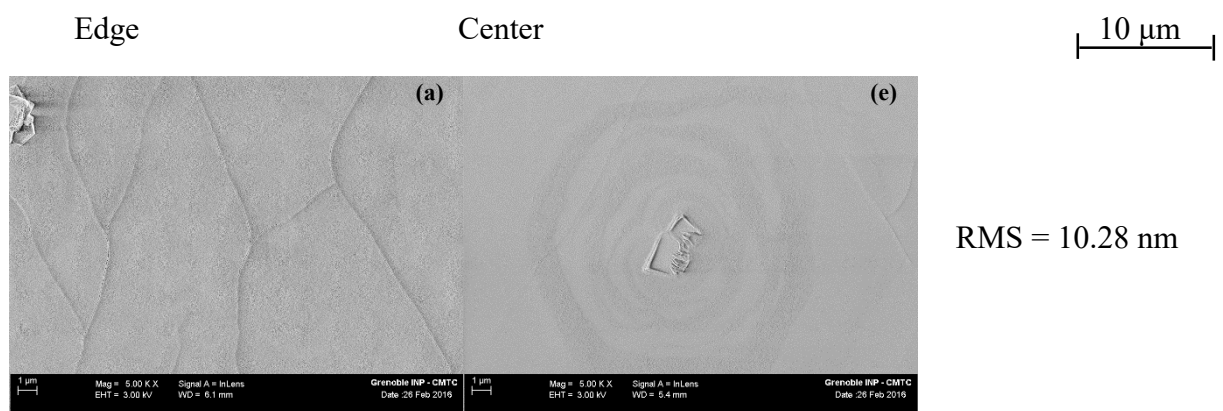
Figure 4.5. ω rocking curve of the AlN-30 with respect to H5

The crystal quality of AlN films has been assessed by XRD with ω rocking curves (Figure 4.5) to estimate the density of dislocations in AlN layers. In fact, the full width at half maximum

(FWHM) values of symmetric (0002) peak, may allow estimation of the screw dislocation densities with respect to the (0001) plane. Similarly, FWHM values of asymmetric ($10\bar{1}2$) or ($10\bar{1}0$) are utilized to assess the density of edge dislocations. It has been investigated that the edge dislocation densities decrease to a limit value while the crystal quality increases. Then, below this value, only screw dislocation could be observed, and its density continues to decrease with the increase of crystal quality.

4.4.2 Surface morphology

In order to assess surface morphology of AlN films, SEM measurements were performed at ambient temperature by utilizing FEG SEM Zeiss ultra 55. In addition, the surface morphology evolution was also characterized by AFM with a Nanoscope equipment (Veeco dimension 3100) operating in tapping mode under ambient conditions. Surface morphologies of AlN layers for AlN films AlN-08, AlN-09, AlN-10, AlN-25 (relative to R1, R2, R3, R4 respectively) at the edge (a, b, c and d) and at the center (e, f, g and h) are given as Figure 5.3. The corresponding RMS roughness values, originated from AFM images ($10 \times 10 \mu\text{m}^2$ scans) at the wafer center, of these AlN layers are also presented. It is worth noting that the surface morphology and the corresponding RMS roughness values of these four repetitions are similar, which can prove the stability of the experimental process. As shown in Figure 4.6, the surfaces exhibit cracks at the edge of these AlN films. At the center, the surfaces are relatively smoother than at the edge and the AlN islands seems fully coalesced; moreover, grains of different orientations ($\neq (002)$) are observed at the center of a hexagon (the hexagonal c-plane).



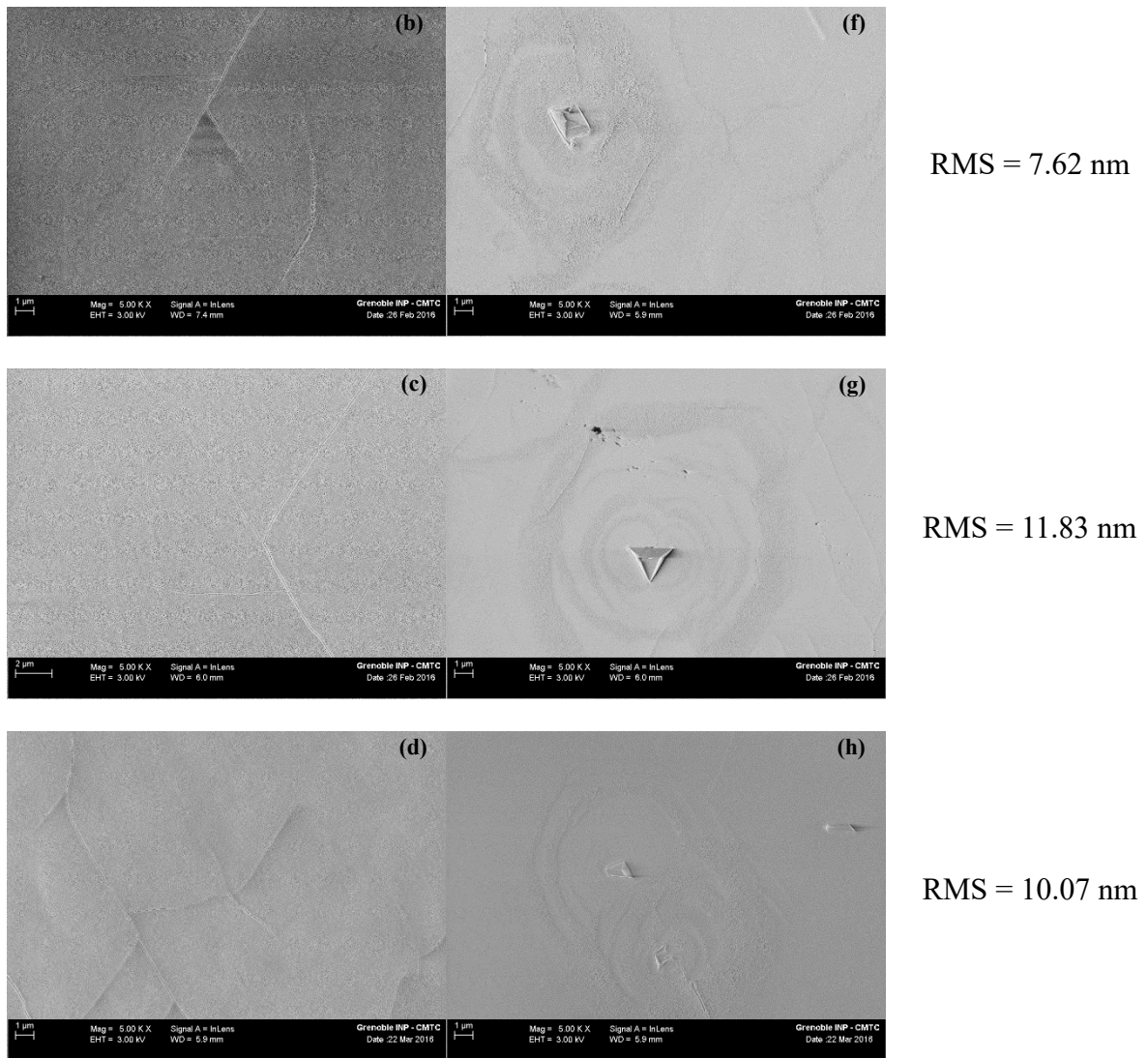


Figure 4.6. Surface morphologies of AlN layers for samples AlN-08, AlN-09, AlN-10, AlN-25 (relative to R1, R2, R3, R4 respectively) at the edge (a, b, c, d) and at the center (e, f, g, h)

In particular, the film surface roughness and grain coarseness can be analyzed. Roughness data were obtained directly from the AFM images by the software Gwyddion whereas the typical surface grain size could be observed by averaging the different values found in the images. In Figure 4.7, two-dimensional $10 \times 10 \mu\text{m}^2$ AFM images at the wafer center for samples AlN-23, AlN-24 and AlN-30 with respect to H13, H14 and H15 respectively (a, b and c); and their corresponding three-dimensional images (d, e and f) are presented. AFM images for other samples are shown in annexes.

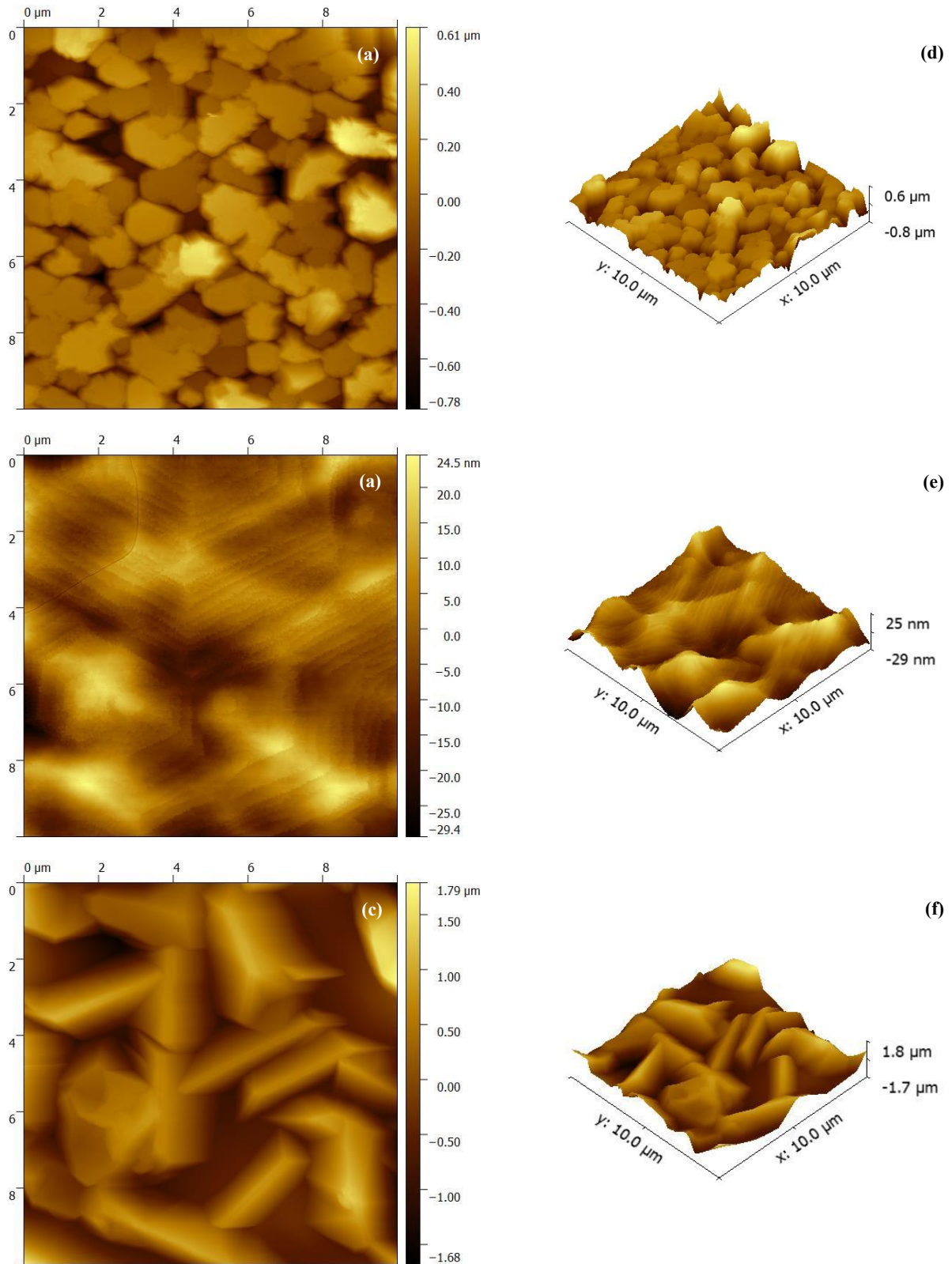


Figure 4.7. AFM images ($10 \times 10 \mu\text{m}^2$ scans) at the wafer center for samples AlN-23 (a and d), AlN-24 (b and e) and AlN-25 (c and f)

AlN-24 is a sample with lower RMS roughness value (7.87 nm) whereas a rough surface

exhibiting improperly coalesced islands is observed for AlN-23 (RMS roughness 192.00 nm). It is worth mentioning that in those samples with lower surface roughness, the AlN islands were coalesced for forming a smoother surface. This observation suggests an influence of island coalescence on surface morphology. The RMS roughness value of AlN-30 is 506.00 nm. It seems that for those polycrystalline (see following section) samples, their surface at the center are extremely rough (RMS roughness > 100 nm). This may due to the large grains located on the surface.

4.4.3 Raman shift

Raman spectroscopy is widely known as a useful, nondestructive and sensitive method for characterizing stress fields in heteroepitaxial layers. The Raman spectrum of obtained AlN samples are measured in backscattering geometry using the 514 nm line of an Ar laser at about 7 mW under room conditions.

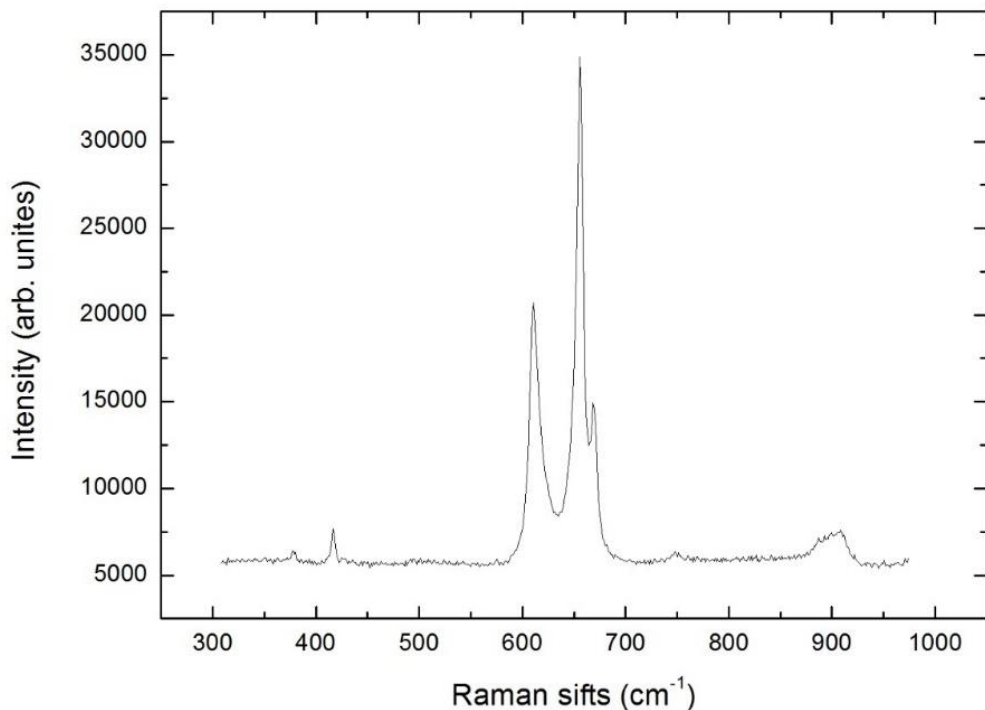


Figure 4.8. Raman spectrum of the sample AlN-30 (relative to H15)

A typical Raman spectrum of all obtained AlN samples is illustrated in Figure 4.8. The most prominent peak observed at about 658 cm^{-1} corresponds to the E_2 (high) phonon mode of AlN, to the biaxial stress in c-plane as well. The two moderate peaks near 614 cm^{-1} , and 670 cm^{-1} are correlated to A_1 (transverse optical mode, TO) and E_1 (TO) modes respectively. The broad peak presented close to 910 cm^{-1} represents the E_1 (longitudinal optical mode, LO). Below 400 cm^{-1} , the small peaks around 376 and 414 cm^{-1} indicate the presents of sapphire substrate.

Currently, the E_2 (high) phonon mode of AlN is studied to deduce the biaxial stress. Yang et al. [51] have found a linear relationship between biaxial stress and Raman shift of AlN E_2 (high) phonon mode: $y = -4.04\sigma + 657.67$. As described before, this stress may take on either sign: for tensile systems, σ is positive while $\sigma < 0$ for compressive systems.

4.4.4 Surface curvature

The surface curvature of AlN samples is measured by a profilometer at ambient temperature. In fact, the total stress of a thin film is the sum of the external stress due to the external loading, the thermally-induced stress and the internal stress (see Chapter 1.2.4). The thermal stress is caused by the mismatch of the thermal expansion coefficients between the grown layer and the substrate, and can be calculated using the following equation^[52]:

$$\sigma_{th} = \frac{E_f}{1-v_f} (\alpha_s - \alpha_f)(T - T_{ref}) \quad (4-3)$$

with T_{ref} the referential temperature, E_f and v_f the Young's modulus and Poisson' ration of the film, as well as α_s and α_f represent the thermal expansion coefficient of the substrate and the film respectively.

In our project, no external load is applied. Thus, σ_{ext} is equal to zero. The stress in grown layers can be estimated by an extensively used analytical solution, the Stoney formula, given as follow^[52]:

$$\sigma = \frac{E_s t_s^2}{6(1-v_s) t_f} \left(\frac{1}{R} - \frac{1}{R_0} \right) \quad (4-4)$$

where E_s the Young's modulus of the substrate, v_s its Poisson's ration and t_s the thickness of the substrate; t_f the thickness of grown films; R and R_0 the curvature radii after and before

deposition respectively, and the difference $\frac{1}{R} - \frac{1}{R_0}$ is the required surface curvature.

However, the Stoney formula requires the respect of following hypotheses:

- The thickness of the deposited film should be smaller than that of the substrate;
- Both the film and substrates are homogeneous, isotropic and linearly elastic;
- The surface curvature $1/R$ is uniform;
- The thickness of the system {substrate + film} should be smaller than its lateral dimensions;

Nevertheless, even the hypotheses are not completely respected, the Stoney stress is used in our work. In convention, if calculated stress is negative, it means that the grown film is in tension; otherwise, the film suffers from compressive stress^[52].

4.4.5 Thickness

The measurements of thickness for every samples are performed by a nulling imaging ellipsometer.

At the end, all values of measured outputs are summarized in Table 4.4.

Table 4.4. Values of each measured responses

	Sample N°	*Order N°	Thick- ness (nm)	Ra roughness at the center (nm)	RMS roughness at the center (nm)	XRD FWHM (arcsec)	Raman shift (cm ⁻¹)	Curva -ture (m ⁻¹)
R1	AlN-08	1	1293.3	7.96	0.28	3576	657.5	-0.037
R2	AlN-09	2	1334.2	6.28	7.62	3684	657.7	-0.035
R3	AlN-10	3	1242.0	8.97	11.83	3311	657.2	-0.032
H1	AlN-11	4	1741.5	31.20	39.20	4087	657.7	-0.052

H2	AlN-12	5	657.9	11.05	17.38	1434	656.6	-0.018
H3	AlN-13	6	145.5	8.50	12.70	779	657.8	-0.006
H4	AlN-14	7	1780.6	242.00	363.00	4206	657.3	-0.083
H5	AlN-28	19	714.1	7.06	8.77	355	649.9	0.013
H6	AlN-16	8	1399.8	15.00	20.80	3077	658.1	-0.041
H7	AlN-17	9	2149.9	12.57	15.47	3889	659.1	-0.058
H8	AlN-18	10	388.5	21.40	39.90	589	651.7	0.011
H9	AlN-19	11	776.4	103.00	171.50	2198	655.7	0.000
H10	AlN-20	12	1226.7	73.00	123.00	1980	656.8	0.004
H11	AlN-21	13	1471.8	10.00	17.10	1130	655.7	0.002
H12	AlN-22	14	1632.2	52.30	121.00	2269	657.4	0.031
H13	AlN-23	15	284.0	142.00	192.00	669	657.2	-0.003
H14	AlN-24	16	2355.5	6.30	7.87	5324	658.0	-0.066
H15	AlN-30	21	836.0	419.00	506.00	1133	653.7	0.023
H16	AlN-26	18	199.0	1.79	2.28	657	644.6	0.010
R4	AlN-25	17	1183.9	8.52	10.07	2091	656.2	-0.029
Ex-1	AlN-29	20	393.5	8.84	11.09	1164	656.4	-0.003

*Experimental order

4.5 Results and discussions with DOE

4.5.1 Influence of each parameter

As mentioned in Chapter 3.2.2, the non-dimensional coefficients of each parameter and the y-intercept coefficient A_0 are calculated by the following equation, and presented afterwards in Table 4.5:

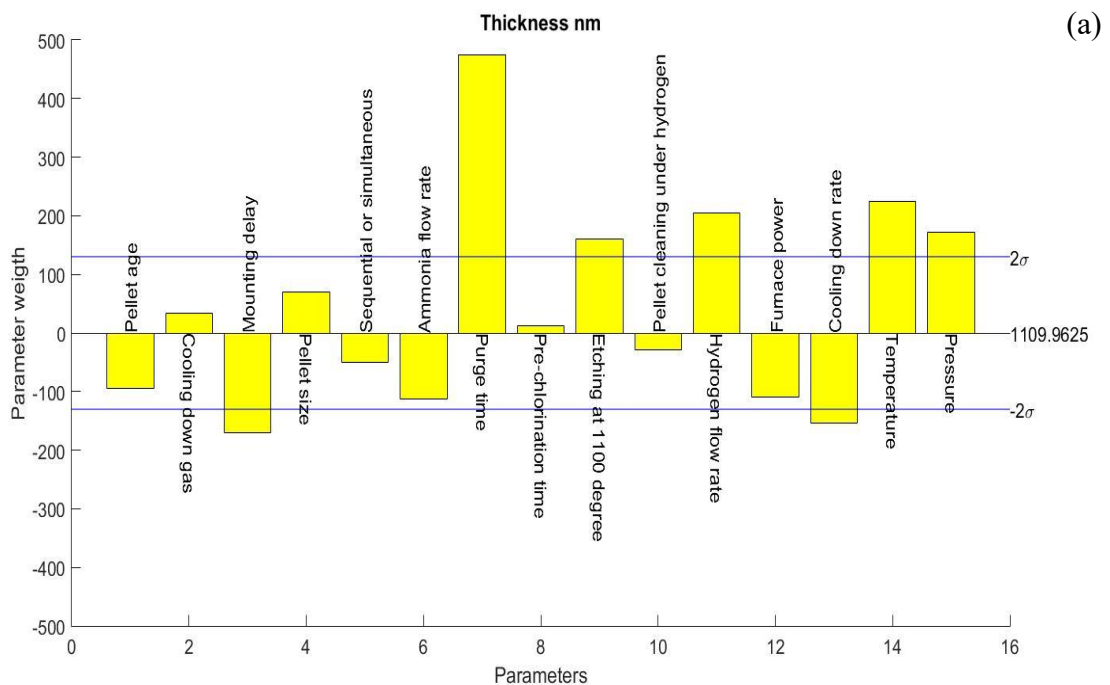
$$A_{i,k} = \frac{1}{n} \sum_{k=1}^n H_n(j,i) \cdot R(j,k) \quad (4-5)$$

Table 4.5. Calculated coefficients of each parameter for measured responses

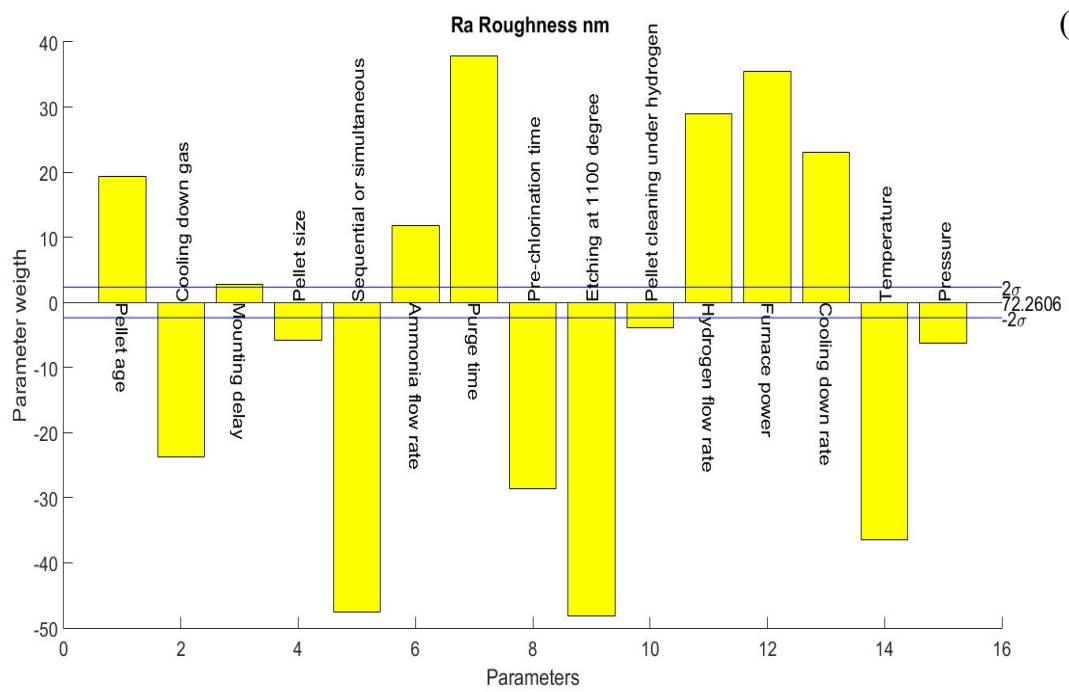
Coefficient	Thickness (nm)	Ra roughness at the center (nm)	RMS roughness at the center (nm)	XRD FWHM (arcsec)	Raman shift (cm ⁻¹)	Curvature (m ⁻¹)
A_0	1110.000	72.261	103.620	2111.000	655.460	-0.015
A_1	-95.063	19.406	16.719	-331.000	0.386	0.004
A_2	34.525	-23.684	-31.058	279.500	0.798	-0.006
A_3	-170.430	2.833	13.583	-232.250	-1.510	0.006
A_4	69.113	-5.879	4.487	149.380	1.425	-0.001
A_5	-50.213	-47.612	-64.704	119.130	-0.545	-0.003
A_6	-112.970	11.866	10.718	-115.130	-0.968	0.005
A_7	474.020	37.911	51.982	1161.900	1.665	-0.016
A_8	12.263	-28.663	-38.971	191.000	0.565	-0.015
A_9	160.590	48.171	-62.337	306.500	-0.291	-0.001
A_{10}	-28.425	-3.836	-12.057	-343.250	-1.232	0.011
A_{11}	204.380	28.984	34.482	239.500	-0.367	-0.004

A ₁₂	-109.960	35.469	38.931	175.130	-0.085	-0.010
A ₁₃	-153.190	23.039	28.202	-288.130	0.855	0.010
A ₁₄	225.200	-36.408	-47.383	312.880	1.225	-0.005
A ₁₅	171.700	-6.316	-7.017	350.880	0.368	-0.013
2σ	130.050	2.353	3.487	1466.500	1.282	0.006

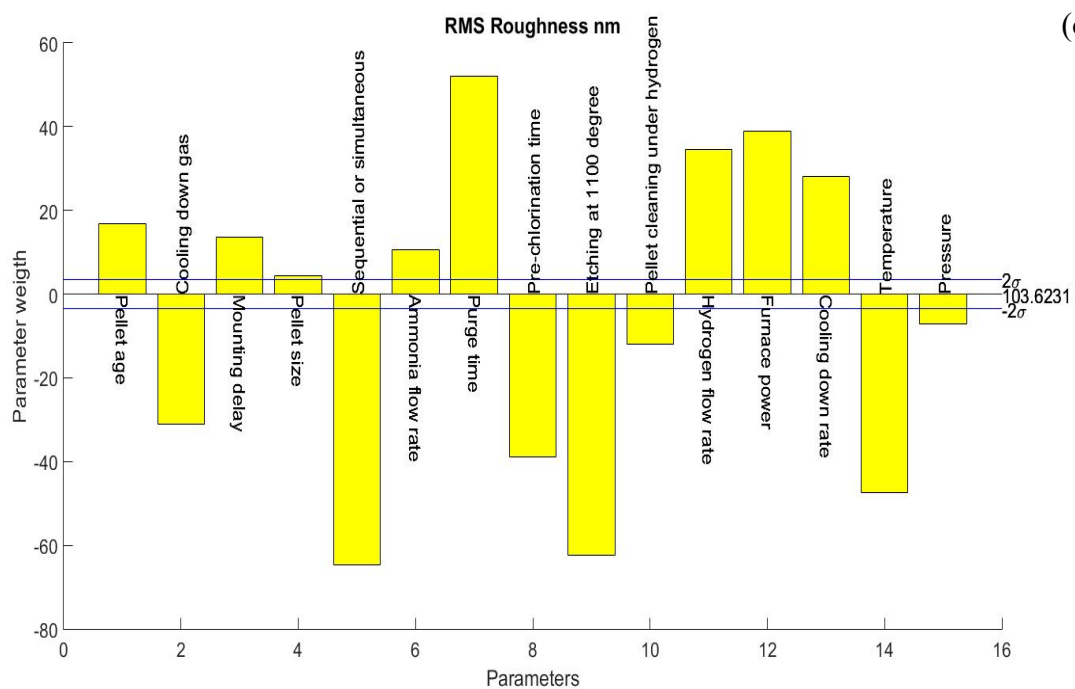
In order to assess the influence of each parameter to a given response, it needs to compare the absolute values of its corresponding calculated non-dimensional coefficient and 2σ . If 2σ is smaller, it means that this parameter has a great impact on the response, and vice versa. Figure 4.9 illustrates the comparison between the absolute values of the 15 chosen deposition parameters and the relative $|2\sigma|$ for each response.



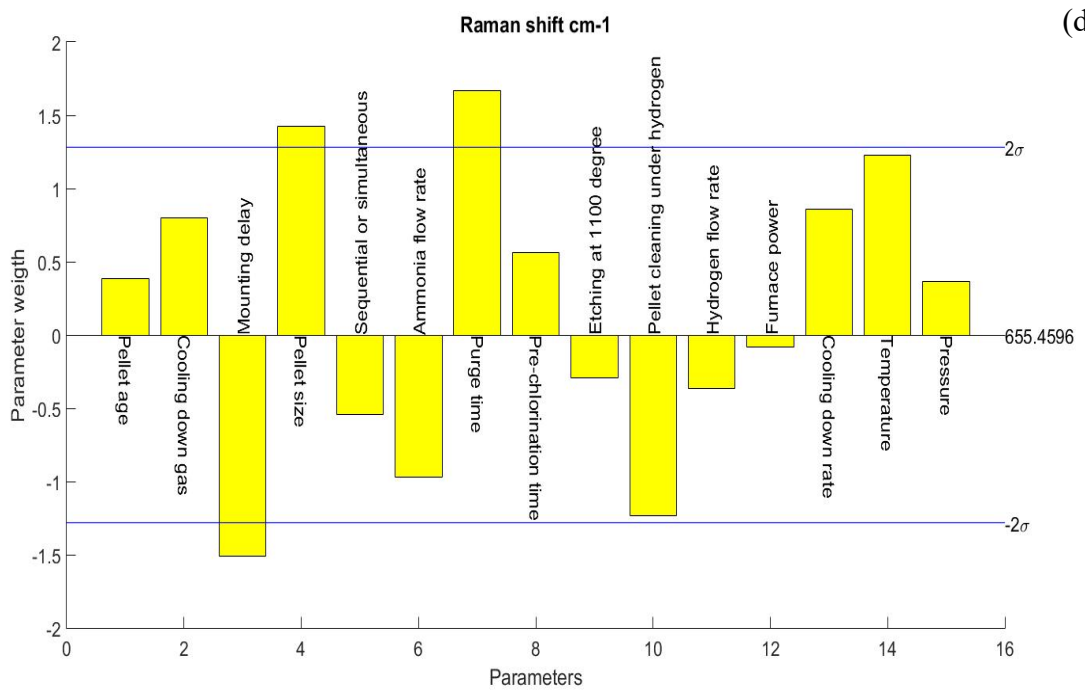
(b)



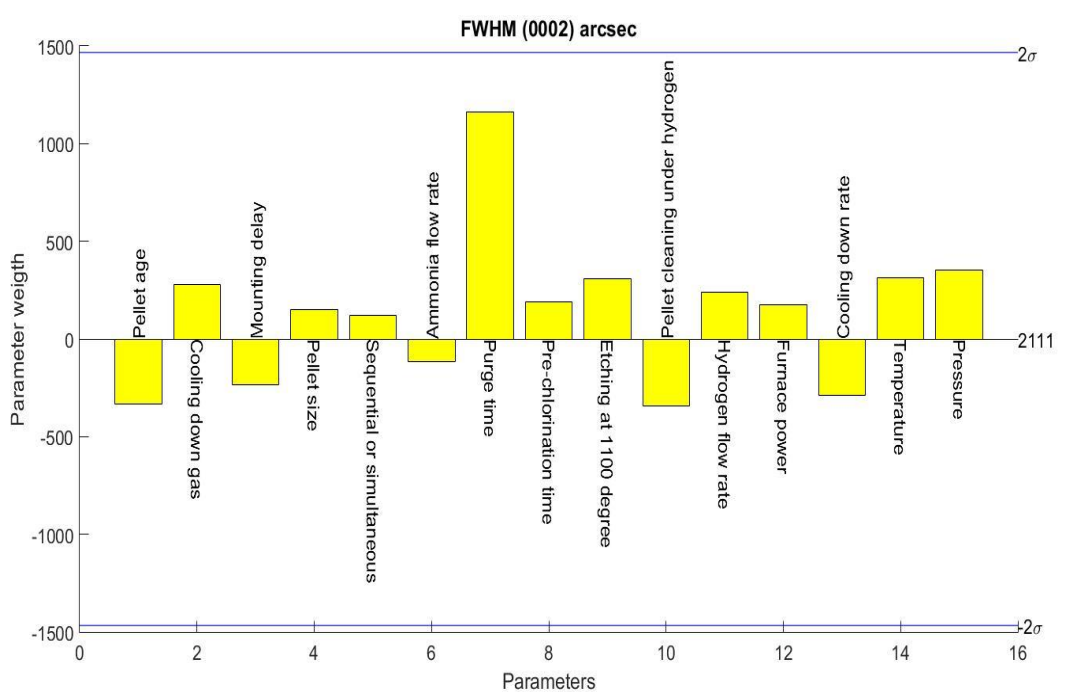
(c)



(d)



(e)



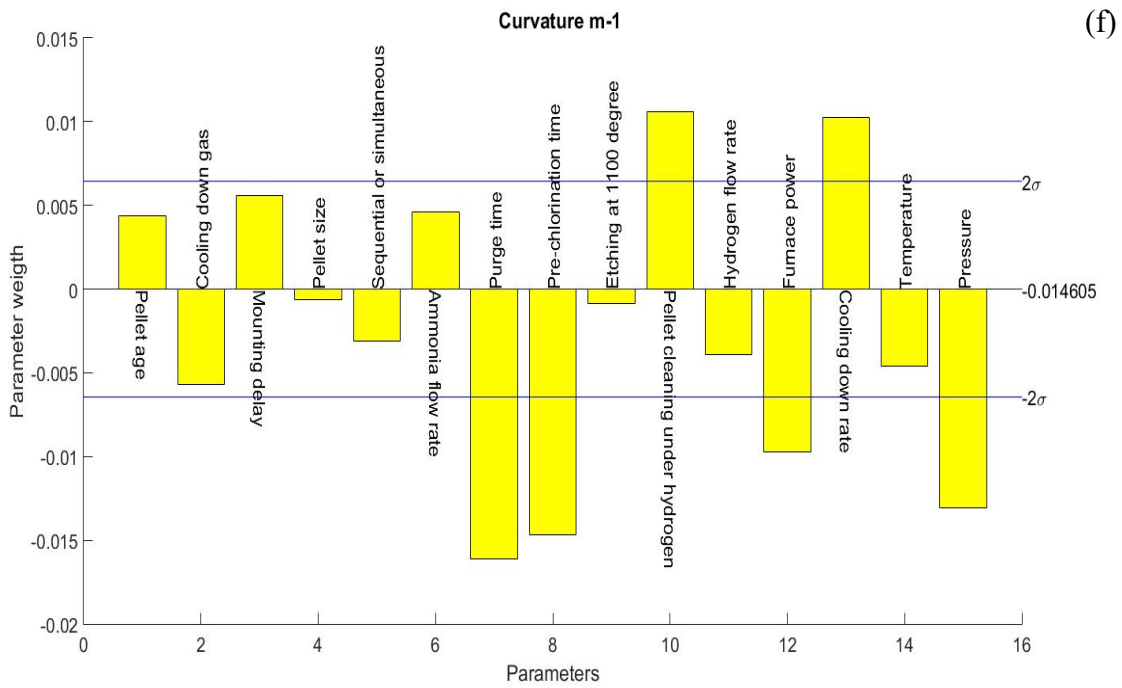


Figure 4.9. Schematic representation of coefficients of every parameter for each response

The influence of each deposition parameter on the measured responses are discussed in the following sections. To simplify the analysis, neglecting the influences of other parameters are negligible while analyzing that of one input. This hypothesis is logical since actually it leads to analyze the parameter through controlling variates.

4.5.1.1 Pellet age

As shown in Figure 4.9, deposition parameters including pellet age, cooling down gas, aluminum flow rate, as well as the gas injection mode affect only the RMS roughness and the Ra roughness.

For ‘pellet age’, the first input parameter, its linear equations for the Ra roughness and the RMS roughness (the second and third response) are written as follow assuming the influences of other parameters are negligible:

$$R_2 = 72.261 + 19.406x_1 \quad (4-6)$$

$$R_3 = 103.620 + 16.719x_1 \quad (4-7)$$

In this case, it can be evidently deduced that the smaller the input value of x_1 is, the smaller values of these two responses are achieved. Therefore, using aluminum pellets which

are used once may lead to a smoother surface (i.e. lower roughness).

4.5.1.2 *Cooling down gas*

Similarly, due to the fact that the relative non-dimensional coefficients of the parameter ‘cooling down gas’ for the RMS roughness and the Ra roughness are negative, and both the absolute values of these two coefficients are smaller than that of their corresponding y-intercept coefficients; cooling down the reactor under 1 slm N₂ can significantly reduce the surface roughness of AlN films.

4.5.1.3 *Gas injection mode*

Even though pulsed flow method is proposed to enhance the migration of aluminum atom on the surface of substrate, and thus lead to a smoother AlN epitaxial layers. However, as shown in Figure 4.9(b) and (c), this parameter ‘gas injection mode’ presents a negative influence on the surface roughness. In this case, the high level, which is the simultaneous gas injection mode, is capable of obtaining a better surface morphology.

4.5.1.4 *Ammonia flow rate*

The same as the above parameters, it can be rapidly found that a higher ammonia flow rate induces a rougher surface of AlN films. In fact, the ratio of N/Al depends on the ammonia flow rate with the following relationship according to the principle reactions in CVD reactors for depositing AlN:

$$\frac{N}{Al} = \frac{v(NH_3)}{v(AlCl_3)} = \frac{v(NH_3)}{\frac{2}{3}v(Cl_2)} = \frac{3}{2} \frac{v(NH_3)}{v(Cl_2)} \quad (4-8)$$

where v the flow rate of gases.

Since the flow rate of chlorine is fixed as 2 sccm, the ratio of N/Al equals to 1 while the ammonia flow rate takes the lowest value in the range. That is, a III/V ratio that close to 1 leads to lower surface roughness of grown AlN layers, which is in agreement with the previous work done by SIMAP.

4.5.1.5 *Mounting delay*

The parameter ‘mounting delay’ has been shown to influence the surface roughness, the Raman shift relative to the E₂ (high) phonon mode of AlN and the thickness of AlN films. Similar to the parameter ‘pellet age’, mounting during the day, the -1 value, may reduce the roughness and thus lead to better surface morphology than the day before.

Besides, Figure 4.9(a) presents a negative effect of this parameter on the film thickness. By using analogy of above discussions, it can be deduced that mounting during the day is favorable to obtain a thick film whereas producing a thin AlN film requires the preparation one day before doing the experiment. We do not explain the non-intuitive effect of this parameter on this response even if it is statistically robust.

With the hypothesis that the influences of other parameters are negligible, the linear relationship between the Raman shift for E₂ (high) phonon mode of AlN, the fifth responses, and this parameter is shown as follow:

$$R_5 = 655.46 - 1.510x_3 \quad (4-9)$$

According to this equation, it seems that the E₂ (high) Raman shift would be close to 655.460 cm⁻¹ while the higher level is taken, and vice versa. However, it is worth mentioning that the equation of Raman shift in terms of biaxial stress proposed by Yang et al. gives a biaxial stress coefficient of the E₂ (high) phonon mode of $-4.04 \pm 0.3 \text{ cm}^{-1}/\text{GPa}$ and the stress-free AlN frequency corresponds to 656.67 cm⁻¹. Consequently, a lower value should be taken to achieve a Raman shift near 656.67 cm⁻¹, and thus a AlN film with less stress.

4.5.1.6 *Pellet size*

It is evident that this parameter has measurable influence on surface roughness and Raman shift for E₂ (high) phonon mode. However, the influences are not very significant since the coefficients are close to the corresponding 2σ .

It is worth noting that using large aluminum pellets for synthesis of AlCl₃ can reduce Ra roughness while small size will increase this kind of roughness. In fact, even though Ra roughness could reflect the microscopic geometry in height direction of the surface, it is not suitable for assess too rough or too smooth surface. Therefore, RMS roughness is more reliable

for analysis.

Moreover, equation that explains relationship between pellet size and E₂ Raman shift is:

$$R_5=655.46+1.425x_4 \quad (4-10)$$

Similar to above analysis, when x₄ equals to +1, the value of the response is 656.875 cm⁻¹. Therefore, it can be concluded that large aluminum pellets could reduce residual stress in grown AlN layers.

4.5.1.7 Purge time

It is observed that the parameter ‘purge time’ has significant influences on nearly every response. Similar to the above analysis, a longer purge time under hydrogen would induce a thicker AlN layer while an AlN thin film could be achieved without purge.

In addition, purging with 4 seconds in a cycle will increase the surface roughness. However, since it has been deduced in above section that introducing simultaneously the active gases into the reactor reduce significantly the surface roughness of AlN films, this result seems to give a conclusion that pulse injection growth method does not possess influence on the surface morphology of grown AlN layers when using a HVPE process.

The relative equation for Raman shift and surface curvature are:

$$R_5=655.46+1.665x_7 \quad (4-11)$$

$$R_6=-0.015-0.016x_7 \quad (4-12)$$

Since Yang et al. has proposed a linear relationship between biaxial stress and Raman shift of AlN E₂ (high) phonon mode: $y = -4.04\sigma + 657.67$, and by the use of Stoney formula, these equations can be transformed respectively as follow:

$$\sigma = \frac{-1}{4.04} (1.665x_7 + (655.46 - 657.67)) = -0.412x_7 + 0.547 \quad (4-13)$$

$$\sigma = \frac{E_s t_s^2}{6(1-v_s) t_f} (-0.015 - 0.016x_7) \quad (4-14)$$

These two equations indicate opposite results. From the first one, it is evident than a larger value of x₇ leads to less stress in grown layer; while for the second equation, a smaller value of x₇ may reduce surface curvature and thus induce a nearly stress-free film. However, since Raman spectroscopy is a method for measuring local stress field, the result of surface curvature is more credible. Surface cracking can explain the discrepancy between these parameters.

In this case, it can be concluded that deposition without purge may induce a thin AlN film with smooth surface and less stress.

4.5.1.8 *Pre-chlorination time*

Based on Figure 4.9(b) and (c), the smaller the value of pre-chlorination time is, the larger surface roughness will be obtained. That is, a longer pre-chlorination time leads to a smoother AlN layer.

On the other hand, a shorter pre-chlorination time is shown to reduce the surface curvature of AlN films. Since in Stoney formula, the stress is proportional to the curvature $1/R$, depositing AlN with longer pre-chlorination time would significantly induce stress in grown layers, which may probably affect the crystal quality, and decrease the surface roughness as described before. This result is reasonable, as observing cracks in AlN films with smooth surface is possible. In fact, the pre-chlorination is favorable to obtain an Al-polar buffer layer that leads to a smooth and less corrosive surface.

4.5.1.9 *Etching time under hydrogen at 1100 degree*

Etching at 1100 °C proposes a significant influence on surface morphology as shown in Figure 4.9(b) and (c). The surface roughness increases rapidly while the time for etching decreases. Therefore, the substrate etching is an effective method to obtain smoother AlN layers, which is in good agreement with literature.

Moreover, for the film thickness, according to Figure 4.9(a), this parameter has a similar influence to the purge time's. In consequence, a longer substrate etching time leads to a thicker AlN layer, and contrariwise, shorter etching time can induce thin AlN films.

4.5.1.10 *Pellet cleaning time under hydrogen*

The following equation showing the relationship between the response of surface curvature and the pellet cleaning time under hydrogen:

$$R_6 = -0.015 + 0.011x_{10} \quad (4-15)$$

In this case, the longer the time for cleaning lasts, the smaller surface curvature is, and thus

less stresses were induced in the grown layer based on the Stoney formula.

In addition, it is evident that cleaning aluminum pellets under hydrogen for 30 minutes leads to a smoother AlN layer.

4.5.1.11 Hydrogen flow rate

This parameter possesses an important influence on the surface roughness. It is found that the values of RMS roughness and Ra roughness increase with the increase of hydrogen flow rate. That is, setting hydrogen flow rate at 0.5 slm is favorable to obtain a smooth AlN film.

Moreover, it is shown that a lower hydrogen flow rate decreases the film thickness while a high one leads to a thicker AlN film.

4.5.1.12 Furnace power

The furnace power affects the surface roughness and curvature of AlN films. The influence of this parameter on surface curvature can be transformed as following equation:

$$R_6 = -0.015 - 0.010x_{12} \quad (4-16)$$

Evidently, a low level of this parameter can induce a surface curvature close to 0 which means a stress-free AlN layer. Therefore, furnace operating at 40% power (corresponding to 600 °C) favor the reduction of stress in grown AlN films.

It is worth noting that a low furnace power also leads to a smaller surface roughness.

4.5.1.13 Cooling down rate

From Figure 4.9(a), it can be found that a low cooling down rate leads to the increase of thickness and vice versa.

In Chapter 2.4, a short introduction to the releasing mechanism of stress is presented. The mismatch of thermal expansion coefficients between AlN and sapphire will introduce thermal stress during the cooling down process. This thermal stress could be calculated through following equation:

$$\sigma_{th} = \frac{E_f}{1-\nu_f} (\alpha_s - \alpha_f)(T - T_{ref}) \quad (4-17)$$

Therefore, the thermal stress change rate is relative to the cooling down rate dT/dt .

However, it is worth noting that the stress calculated by the Stoney formula is the residual stress (final stress), but not the thermal stress induced by mismatch of thermal expansion coefficients.

According to Figure 4.9(f), a higher cooling down rate would decrease the value of surface curvature and thus leads to less stress in grown layers based on the Stoney formula.

However, a higher cooling down rate significantly increases the surface roughness. We explain the influence of this parameter by uncontrolled growth after ending of reactant injection, i.e. due to reactor wall desorption of aluminum and nitrogen compounds.

4.5.1.14 *Growth temperature*

The growth temperature has an important influence on the surface morphology of AlN layers. It is evident that high temperature will induce smooth surface.

Moreover, for the film thickness, according to Figure 4.9(a), higher growth temperature favors the increase of film thickness while lower temperature leads to the growth of thin films.

4.5.1.15 *Total pressure*

This parameter has a significant effect on the surface curvature. Indeed, a lower pressure could reduce surface curvature and leads to reduction of residual stress in heteroepitaxial AlN layer. However, deposition under low pressure would increase surface roughness according Figure 4.9(b) and (c).

4.5.2 Accuracy of the linear model without interactions

According to the Chapter 3.2.3, it is necessary to verify the accuracy of this linear model at the boundaries and the center of experimental domain. Therefore, by using MATLAB, the difference between the theoretical value calculated by the model and the experimental data of ‘-1 experiment’ for each response are summarized in the following table:

Table 4.6. Theoretical value and experimental data of ‘-1 experiment’

Response	$R_{\text{theoretical, exp-1}}$	$R_{\text{-1 experiment'}}$	Difference	2σ
----------	---------------------------------	-----------------------------	------------	-----------

Thickness	478.42	393.5	84.925	130.05
Ra roughness	113.32	8.84	104.48	2.3532
RMS roughness	168.05	11.09	156.96	3.4807
XRD FWHM	135	1164	-1029	1466.5
Raman shift	653.17	656.39	-3.215	1.2815
Curvature	0.022308	-0.0031465	0.0254545	0.0064418

It is evident that for most of the responses, including RMS roughness, Ra roughness, Raman shift for E₂(high) and surface curvature, the absolute value of difference between the theoretical value and experimental data is larger than 2σ . Based on the post-treatment method presented in Chapter 3.2.3, the presence of interactions in the linear model for these responses is indicated. Moreover, the calculated differences for the two responses of surface roughness, are nearly 50 times larger than the corresponding 2σ value, which seems the presence of strong interactions between growth parameters.

For simplification, here we called the influence of each parameter on the responses in the linear model without interactions as ‘main effect’. The response surface should be a linear surface in multi-dimensional space with this simplest model. However, the strong interactions between parameters could not be neglected since they would significantly twist the linear response surface mentioned before, or even conceal the main effects.

In this case, it is necessary to determine the non-dimensional coefficients of these interactions and thus study their influences on the responses. However, for 15 parameters, it needs 2^{16} experiments to completely determine all coefficients, which is a waste of time and money. Therefore, two methods are proposed:

The first one is to consider only the first and second order interactions while neglecting all high-order interactions. This is with respect to the principle idea of fractional factorial design, which can reduce the number of experiments. The main drawback is that the total number of supplementary experiments could be as high as $2^{16}-16$ if every interaction plays a role.

The second method relies on the neglect of parameters that seem to have no measurable influence on responses. By reducing the number of parameters, it is possible to determine all

coefficient of a linear model with interactions using less experiments.

For the two responses, thickness and XRD FWHM, without presence of interactions in the linear model, it is necessary to verify the accuracy at the center of experimental domain. Results are presented in Table 4.7.

Table 4.7. Theoretical value and average experimental data of ‘central’ experiments

Response	$R_{\text{theoretical, central}}$	$R_{\text{'central experiment'}}$	Difference	2σ
Thickness	860.1	1263.3	-403.25	130.05
Ra roughness	1558.8	3165.5	-1606.8	1466.5

Evidently, the nonlinear terms should be added in the model since for each of these two responses, the absolute value of difference are larger than that of 2σ . Similarly, the nonlinear effect twists the response surface as well.

In general, interactions between parameters and nonlinear terms are observed. Consequently, the linear model without interactions could not describe their effects on the responses. The next step is to construct a new and more complex model so that these influences could be determined. Whatever the lack of accuracy of the linear model without interactions, the screening method indicates if a parameter has an influence or not, which is in the particular case of this study crucial for the future works. Also, it is clear that other parameters, that have to be determined, play a strong role. For example, the crystal quality is strongly variable but the main parameters influencing it are not highlighted by this screening. This is counter intuitive but statistically robust. It will oblige us to change the design of our experimental apparatus or our recipe.

4.5.3 Validation

Assuming that an accurate model is finally found, validation of this model should be done to assess its confidence through statistic tools.

Due to the fact that transformation of response can expand or contract the scale of responses and improve the independence of average of experiments versus the variance,

transformations are generally used before the assessment. Statistic tools like residual analysis are always utilized for estimating the confidence of model.

However, it takes long time for transforming responses, constructing a more complex model and making more experiments. For instant, we preliminarily analyzed the main effects of each parameter on every response due to the time limit, and plan to study the interactions and nonlinear terms based on recent results.

5. Conclusions and perspectives

As one of the III-nitride semiconductors, AlN presents many interesting properties including wide band gap, high electron mobility, good mechanical hardness, stable chemical properties and excellent thermal stability and has been proposed as a promising material for many potential applications such as optoelectronics and microelectronics. In nuclear industry, since its good diffusion barrier properties, it seems to be a possible coating material for reducing fuel-cladding interaction and inter-diffusion. Moreover, it is also a candidate for non-destructive evaluation in nuclear reactors due to its radiation resistance.

However, even though researches on AlN have been significantly increased in recent years, it is still difficult to produce high crystal quality AlN in industry-grade, which leads to limit the development of AlN-based devices. Therefore, study of heteroepitaxial growth mechanism of AlN and optimizations of its growth process, allow to improve the crystal quality

In consequence, this internship project aims to assess the influence of growth conditions of a high temperature hydride vapor phase epitaxy process on the AlN crystal quality by a design of experiment method using a Hadamard matrix H_{16} . The main results are presented as follow:

1. Current experimental designs for studying AlN are mostly based on the idea that varying a parameter at one time, and thus require high time and economic costs. According to the principle concept of optimization, our study concerns the correlation of deposition process to AlN crystal defects using a design of experiment method so that more experimental information could be provided with less number of experiments;
2. Combining with characterization methods including scanning electron microscopy, atomic force microscopy, X-ray diffraction, Raman spectroscopy, profilometry and ellipsometry, we study characteristics relative to heteroepitaxial growth quality such as thickness, residual stress, surface roughness and dislocation densities of obtained samples;
3. Through a linear model without interactions and a Hadamard matrix H_{16} , we analyzed the measurable influence of parameters on each response;

4. Based on the constructed linear model, we compared the theoretical value and experimental data, and observe interactions between parameters and presence of nonlinear terms.

According to recent results, sequential studies can be expected:

1. It is possible to analyze the influence of growth conditions on physicochemical and electrical properties of AlN by corresponding characterizations of obtained samples;
2. Determination of the effects of observed interactions and nonlinear terms and validation of the final model provide the possibility to optimize current HT-HVPE process;
3. The characterization method transmission electron microscopy allows more precise observation of dislocations and other crystal defects, can be used for in the next step of study.

6. References

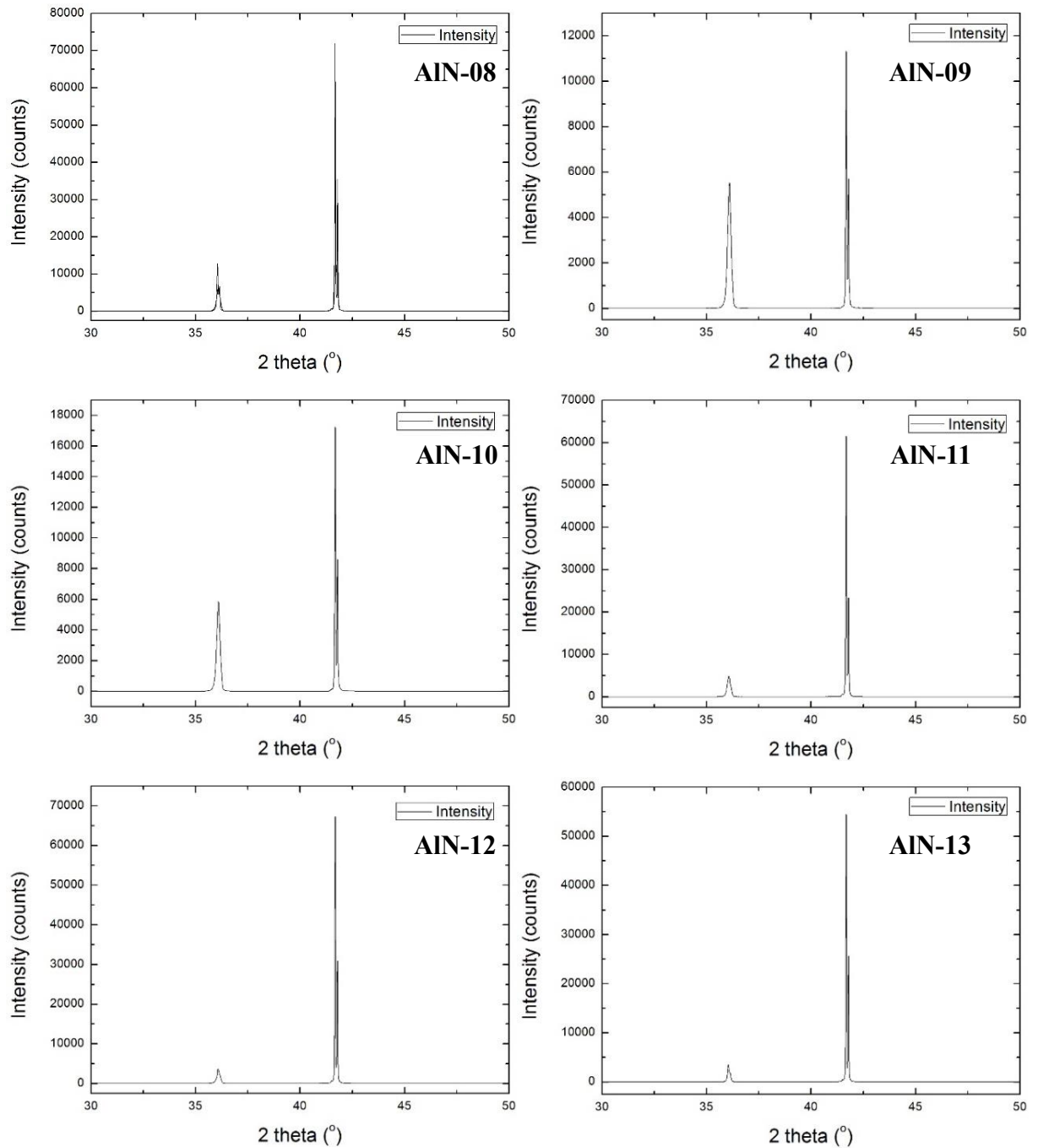
- [1] Coudurier N. Contribution à l'épitaxie des nitrures d'aluminium et de bore par dépôt chimique en phase vapeur à haute température[D]. Université de Grenoble, 2014.
- [2] Henini M, Razeghi M. Optoelectronic Devices: III Nitrides[M]. Elsevier, 2004.
- [3] 李言荣.电子材料导论[M].北京：清华大学出版社,2001.
- [4] 姜复松, 陈宏伟.讯息传输材料.台湾：五南图书出版股份有限公司,2004.
- [5] 田民波.材料学概论[M].台湾：五南图书出版股份有限公司,2015.
- [6] Kamber D S. Hydride vapor phase epitaxy of aluminum nitride[M]. ProQuest, 2008.
- [7] Claudel A. Elaboration et caractérisation de couches de nitre d'aluminium AlN par CVD haute température en chimie chlorée[D]. Institut National Polytechnique de Grenoble-INPG, 2009.
- [8] 任凡.高质量 AlN 材料分子束外延生长机理及相关材料物性研究[D].清华大学电子工程系,2010.
- [9] Polarization effects in semiconductors: from ab initio theory to device applications[M].Springer Science & Business Media, 2007.
- [10] Crystal Growth and Characterization of Advanced Materials[M].World Scientific, 1988.
- [11] Springer handbook of electronic and photonic materials[M].Springer Science & Business Media, 2006.
- [12] Oda O.Compound semiconductor bulk materials and characterizations[M]. Singapore/Hackensack: World Scientific, 2007.
- [13] Florescu D I, Asnin V M, Pollak F H. Thermal conductivity measurements of GaN and AlN[J]. Compound Semiconductor, 2001, 7(2): 62-67.
- [14] W. M. Yim and R. J. Pa. Thermal expansion of AlN, sapphire, and silicon. Journal of Applied Physics, 45(3) :14561457, 1974.
- [15] Y. Goldberg. Properties of Advanced Semiconductor Materials GaN, AlN, InN, BN, SiC, SiGe. John Wiley & Sons, 2001.
- [16] K. Tsubouchi and N. Mikoshiba. Zero-temperature-coe cient SAW devices on AlN epitaxial lms. Sonics and Ultrasonics, IEEE Transactions on, 32(5) :634 644, 1985.
- [17] S. Adashi. Properties of Group-IV, III-V and II-VI Semiconductors. Wiley, 2005.
- [18] 陈秀文. AlN 薄膜外延生长及光电性能研究[D]. 河南大学, 2013.
- [19] W. Fincham, M. H. Freeman. Optics[M]. London: Butterworths, 1980
- [20] Taniyasu Y, Kasu M, Makimoto T. An aluminium nitride light-emitting diode with a wavelength of 210

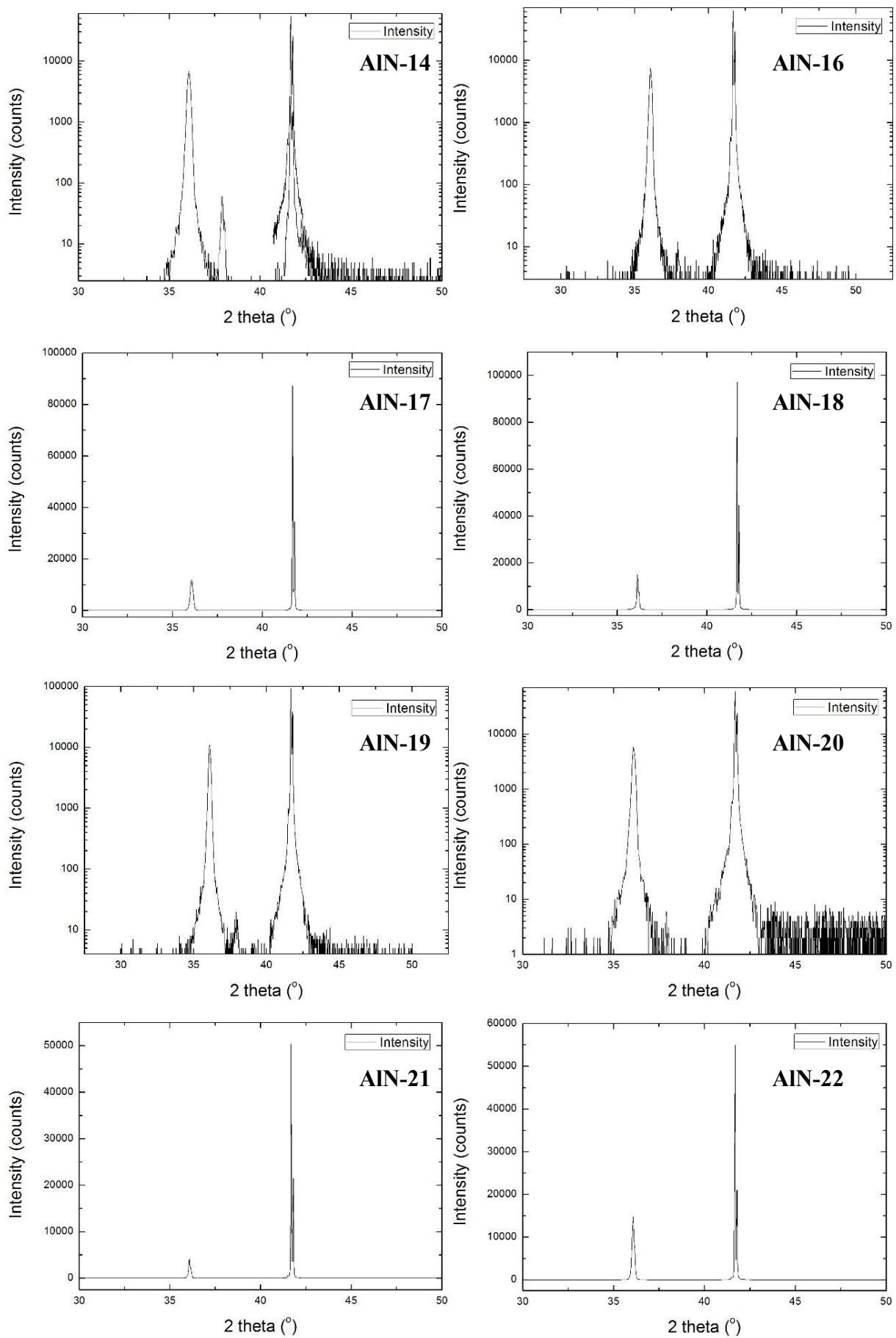
- nanometres[J]. Nature, 2006, 441(7091): 325-328.
- [21] Akasaki I, Amano H, Nakamura S. Blue LEDs—Filling the world with new light[J]. The Nobel Prize In Physics, 2014.
- [22] 张进城, 王冲, 杨燕, 等. AlN 阻挡层对 AlGaN/GaNHEMT 器件的影响[J].
- [23] 一凡. AlGaN/AlN/GaN 大功率微波 HEMT[J]. 微电子技术, 2003, 31(5):8-8.
- [24] Kim I, Khatkhatay F, Jiao L, et al. TiN-based coatings on fuel cladding tubes for advanced nuclear reactors[J]. Journal of Nuclear Materials, 2012, 429(1 - 3):143–148.
- [25] Khatkhatay F, Jian J, Jiao L, et al. Diffusion barrier properties of nitride-based coatings on fuel cladding[J]. Journal of Alloys & Compounds, 2013, 580(8):442-448.
- [26] Kim I, Khatkhatay F, Jiao L, et al. TiN-based coatings on fuel cladding tubes for advanced nuclear reactors[J]. Journal of Nuclear Materials, 2012, 429(1 - 3):143–148.
- [27] Massih A R. Models for MOX fuel behaviour[J]. A selective review, SKI Report, 2006, 10.
- [28] Massih A R, Forsberg K. Calculation of grain boundary gaseous swelling in UO₂[J]. Journal of Nuclear Materials, 2008, 377(2): 406-408.
- [29] 白新德.材料腐蚀与控制[M]. 清华大学出版社有限公司, 2005.
- [30] Parks D, Tittmann B. Radiation tolerance of piezoelectric bulk single-crystal aluminum nitride.[J]. IEEE Transactions on Ultrasonics Ferroelectrics & Frequency Control, 2014, 61(7):1216-1222.
- [31] 李田, 谢杰, 杨成. 超声技术在核电无损检测领域的适应性发展[J]. 科技视界, 2014(12):267-268.
- [32] Tittmann B R, Reinhardt B, Parks D. Nuclear radiation tolerance of single crystal Aluminum Nitride ultrasonic transducer[C]// Ultrasonics Symposium. IEEE, 2014:609-613.
- [33] III-Nitride Ultraviolet Emitters: Technology and Applications[M]. Springer, 2015.
- [34] Jones A C, Hitchman M L. Chemical vapour deposition: precursors, processes and applications[M]. Royal Society of Chemistry, 2009.
- [35] 陈一仁. Al_xGa(1-x)N 和 AlN/GaN 材料的 MOCVD 生长与器件研究[D]. 中国科学院研究生院(长春光学精密机械与物理研究所), 2014.
- [36] Kansas State University. Department of Physics. MOCVD Growth and Characterization of Aluminum-rich Aluminum Nitride/aluminum Gallium Nitride Epilayers and Quantum Wells[M]. ProQuest, 2007.
- [37] Boichot R, Coudurier N, Mercier F, et al. Epitaxial growth of AlN on c-plane sapphire by High Temperature Hydride Vapor Phase Epitaxy: Influence of the gas phase N/Al ratio and low temperature protective layer[J]. Surface and Coatings Technology, 2013, 237: 118-125.

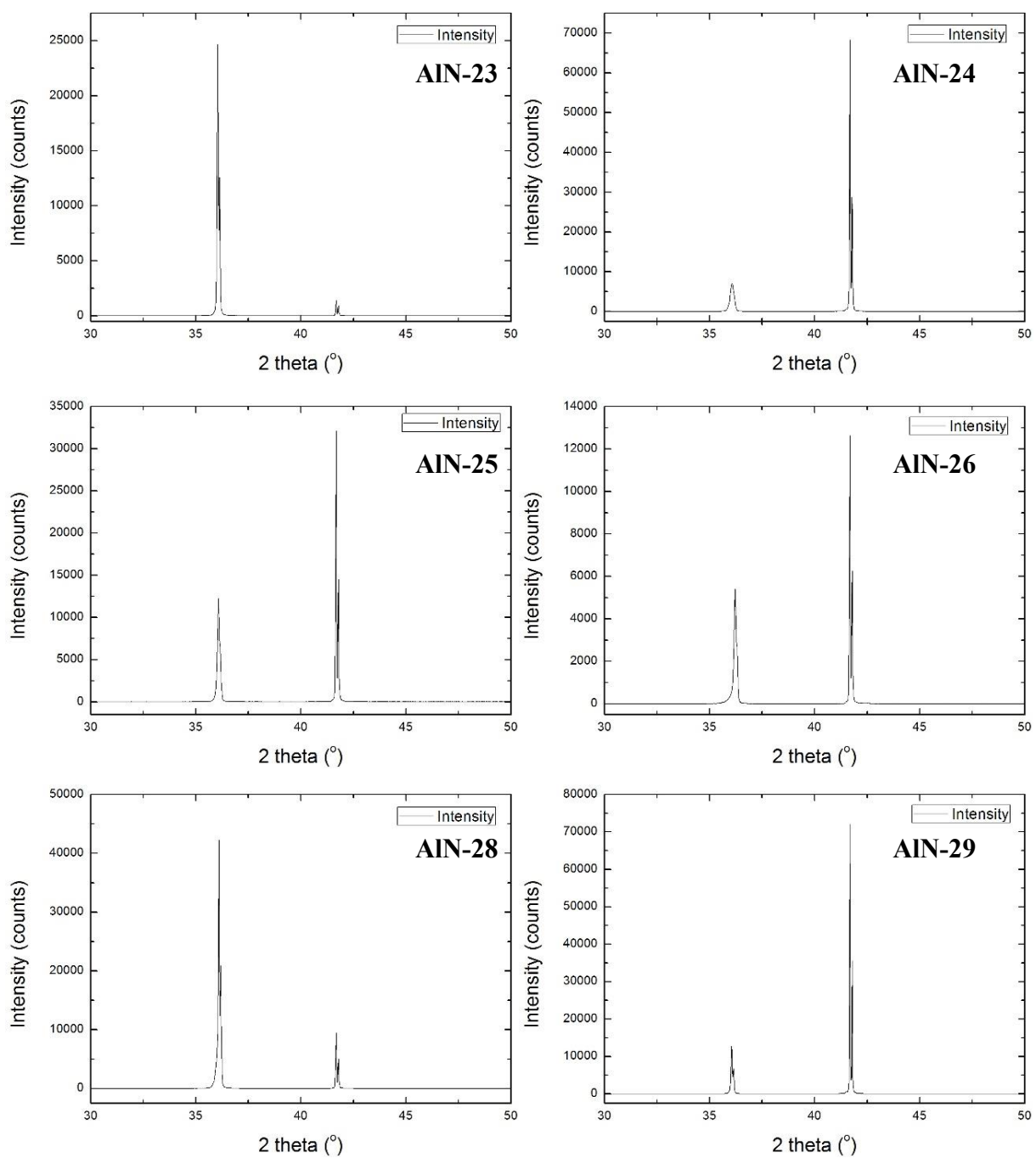
- [38] P. Pascal. Tome VI (B, Al, Ga, In, Th). Nouveau Traite de Chimie Minerale, 1961.
- [39] Amano H, Sawaki N, Akasaki I, et al. Metalorganic vapor phase epitaxial growth of a high quality GaN film using an AlN buffer layer[J]. Applied Physics Letters, 1986, 48(5): 353-355.
- [40] 张洁, 彭铭曾, 朱学亮, 等. AlN 外延薄膜的生长和特征[J]. 激光与红外, 2007, 37(B09): 974-976.
- [41] Nakarmi M L, Cai B, Lin J Y, et al. Three-step growth method for high quality AlN epilayers[J]. physica status solidi (a), 2012, 209(1): 126-129.
- [42] Kumagai Y, Yamane T, Miyaji T, et al. Hydride vapor phase epitaxy of AlN: thermodynamic analysis of aluminum source and its application to growth[J]. physica status solidi (c), 2003 (7): 2498-2501.
- [43] Boichot R, Coudurier N, Mercier F, et al. CFD modeling of the high-temperature HVPE growth of aluminum nitride layers on c-plane sapphire: from theoretical chemistry to process evaluation[J]. Theoretical Chemistry Accounts, 2014, 133(1): 1-13.
- [44] Pons M, Boichot R, Coudurier N, et al. High temperature chemical vapor deposition of aluminum nitride, growth and evaluation[J]. Surface and Coatings Technology, 2013, 230: 111-118.
- [45] Balaji M, Claudel A, Fellmann V, et al. Effects of AlN nucleation layers on the growth of AlN films using high temperature hydride vapor phase epitaxy[J]. Journal of Alloys and Compounds, 2012, 526: 103-109.
- [46] Coudurier N, Boichot R, Fellmann V, et al. Effects of the V/III ratio on the quality of aluminum nitride grown on (0001) sapphire by high temperature hydride vapor phase epitaxy[J]. physica status solidi (c), 2013, 10(3): 362-365.
- [47] 徐永宽, 李强, 程红娟, 等. HVPE 法生长 AlN 薄膜材料[J]. 微纳电子技术, 2010 (2): 89-92.
- [48] Francis Baillet. Plan d'expérience[M]. Grenoble-INP Phelma, 2015.
- [49] Soomro A M, Wu C, Lin N, et al. Modified pulse growth and misfit strain release of an AlN heteroepilayer with a Mg–Si codoping pair by MOCVD[J]. Journal of Physics D: Applied Physics, 2016, 49(11): 115110.
- [50] Ayers J E. Heteroepitaxy of semiconductors: theory, growth, and characterization[M]. CRC press, 2007.
- [51] Yang S, Miyagawa R, Miyake H, et al. Raman scattering spectroscopy of residual stresses in epitaxial AlN films[J]. Applied physics express, 2011, 4(3): 031001.
- [52] Isselé H. Caractérisation et modélisation mécaniques de couches minces pour la fabrication de dispositifs microélectroniques-application au domaine de l'intégration 3D[D]. Grenoble, 2014.

7. Annex

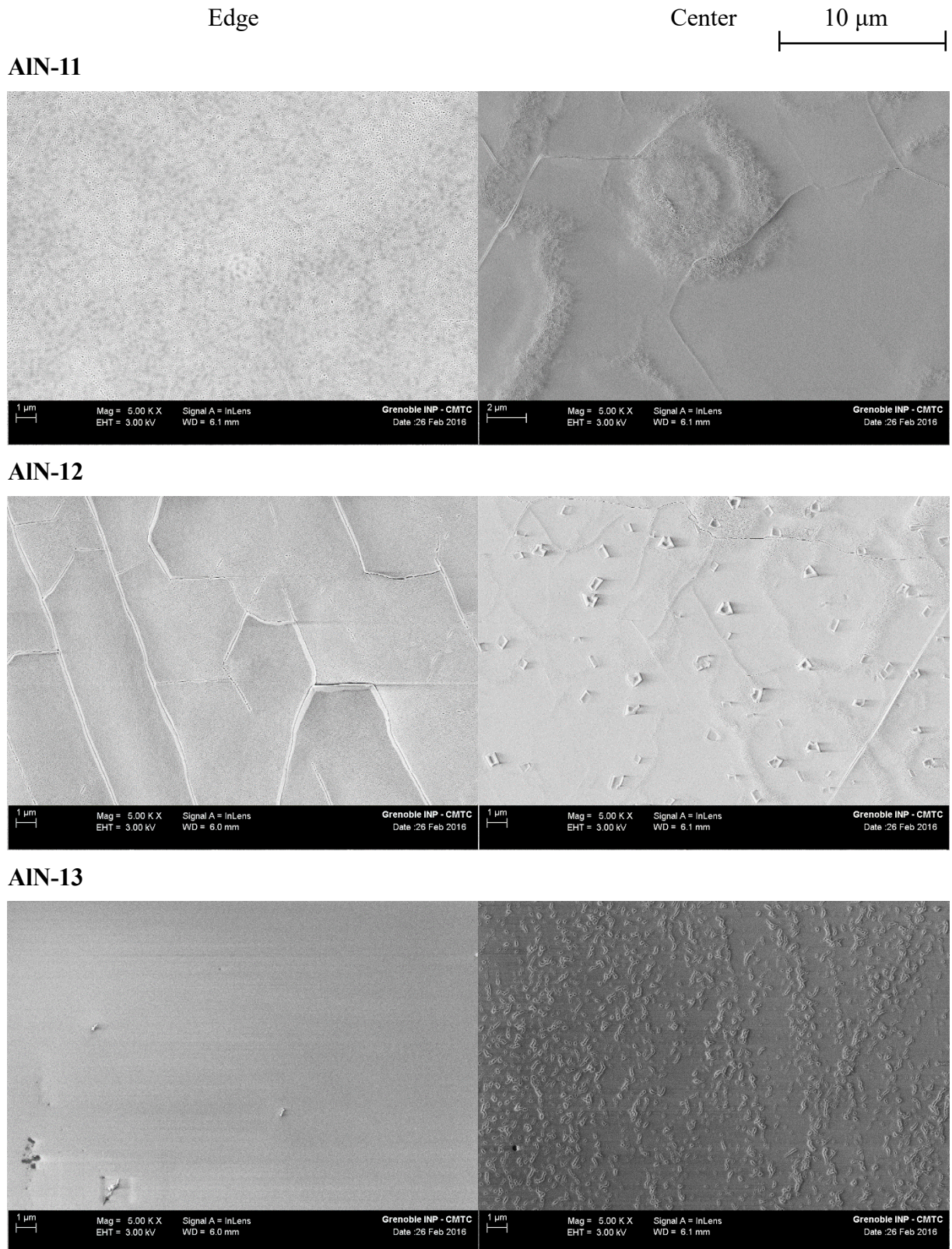
7.1. $2\theta-\omega$ XRD spectrum for each sample

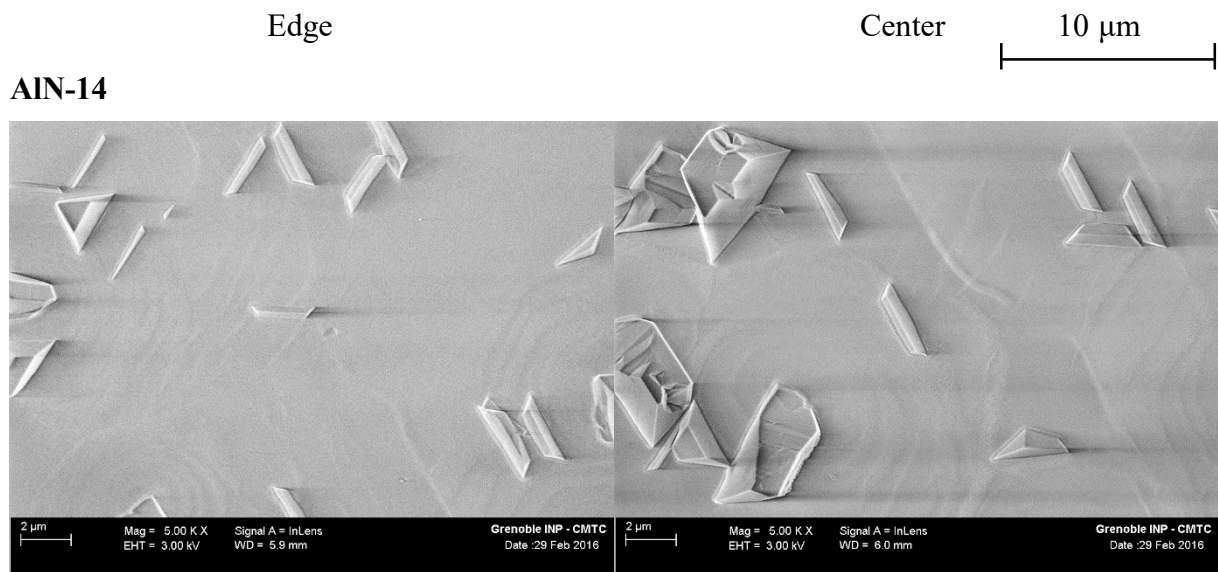




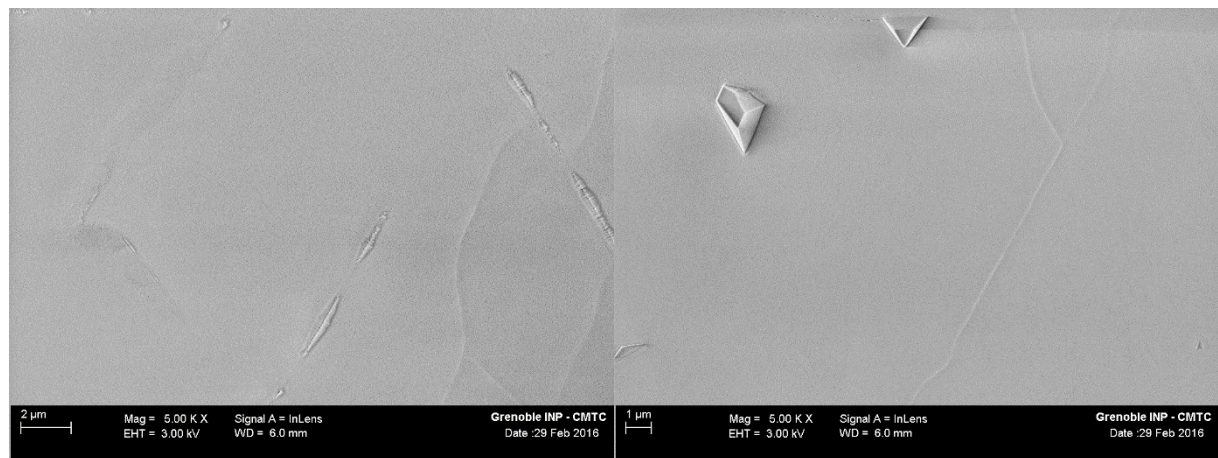


7.2. SEM images for each sample

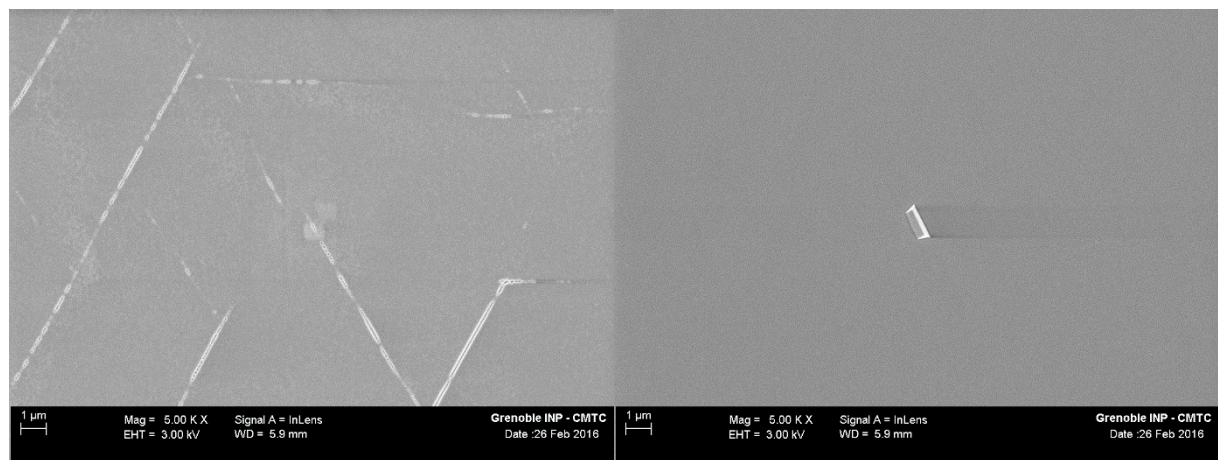


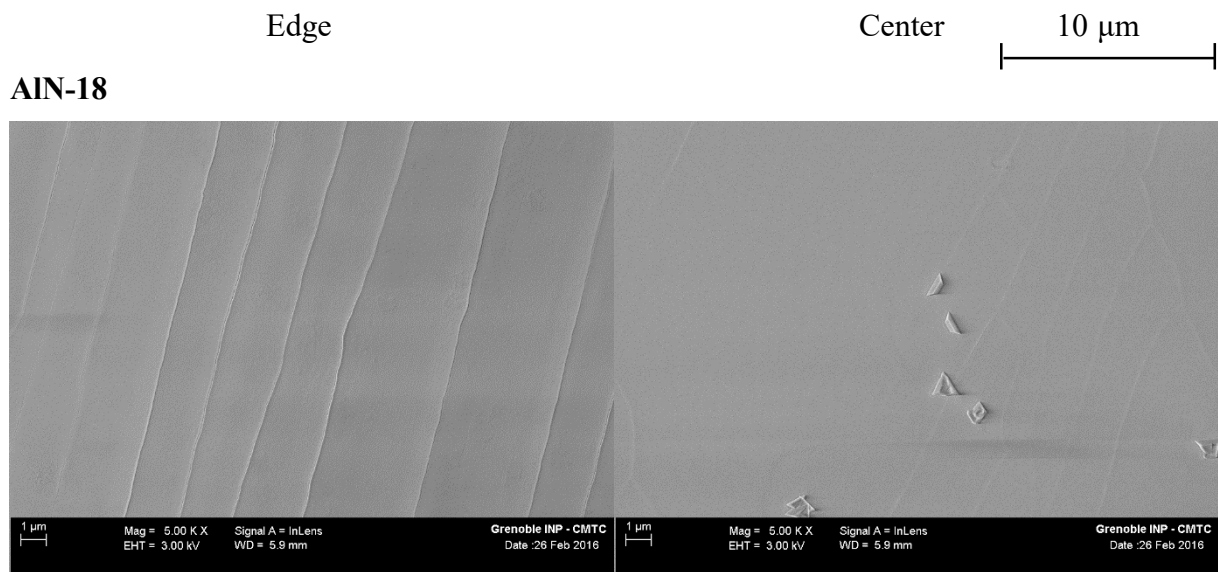


AIN-16

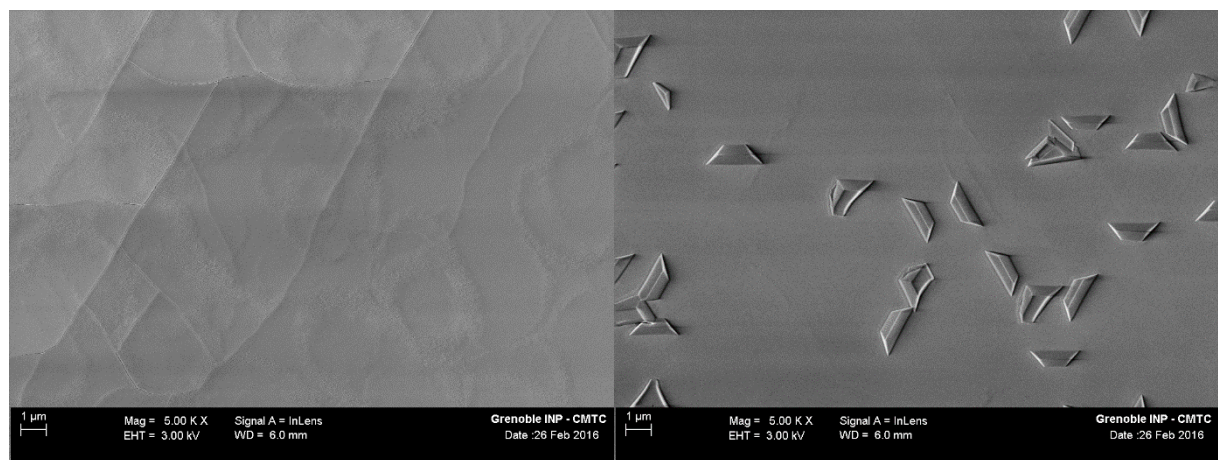


AIN-17

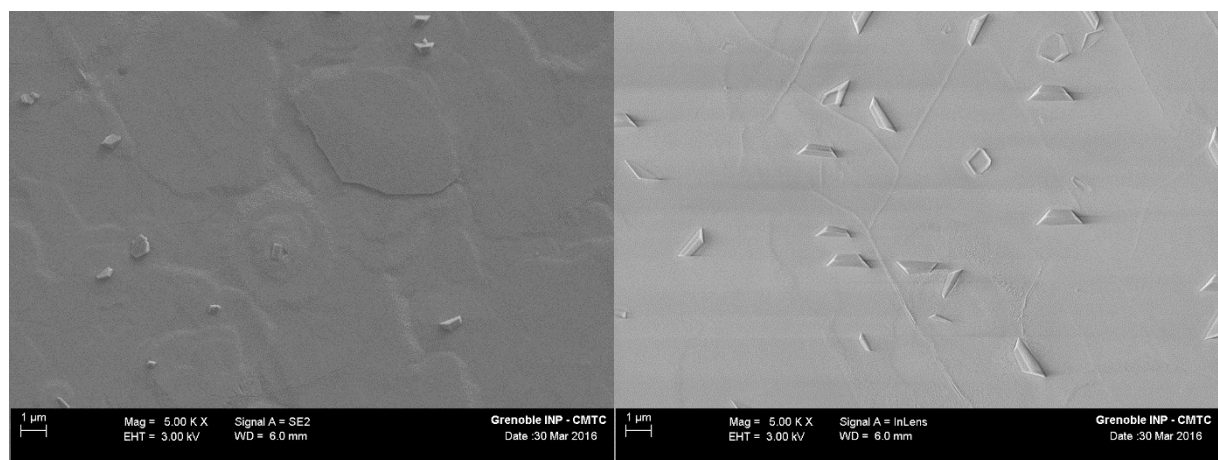


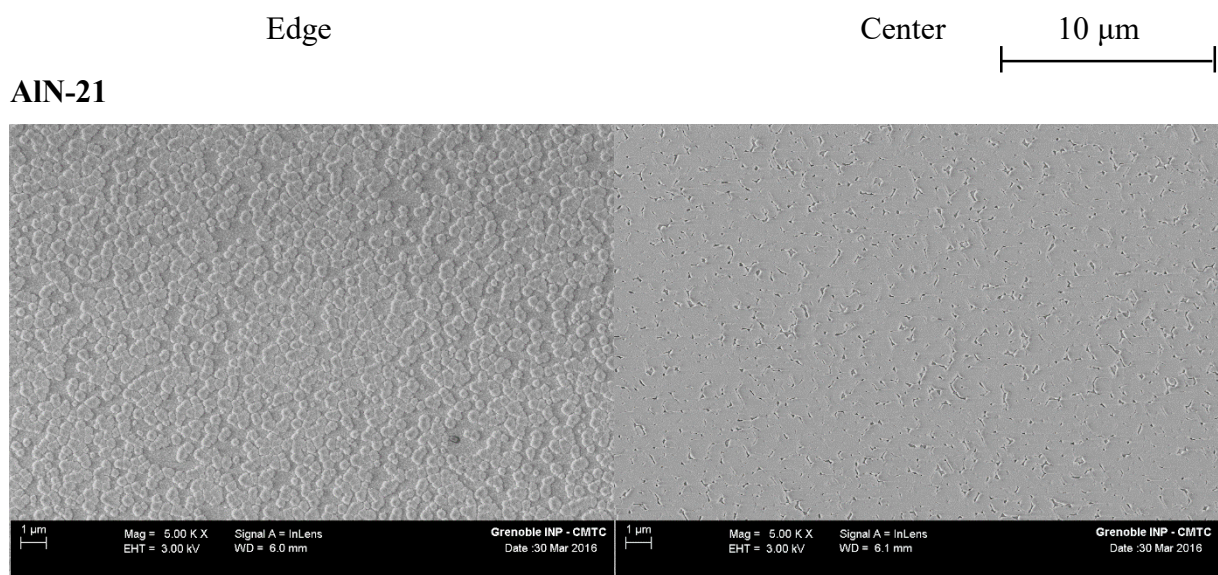


AIN-19

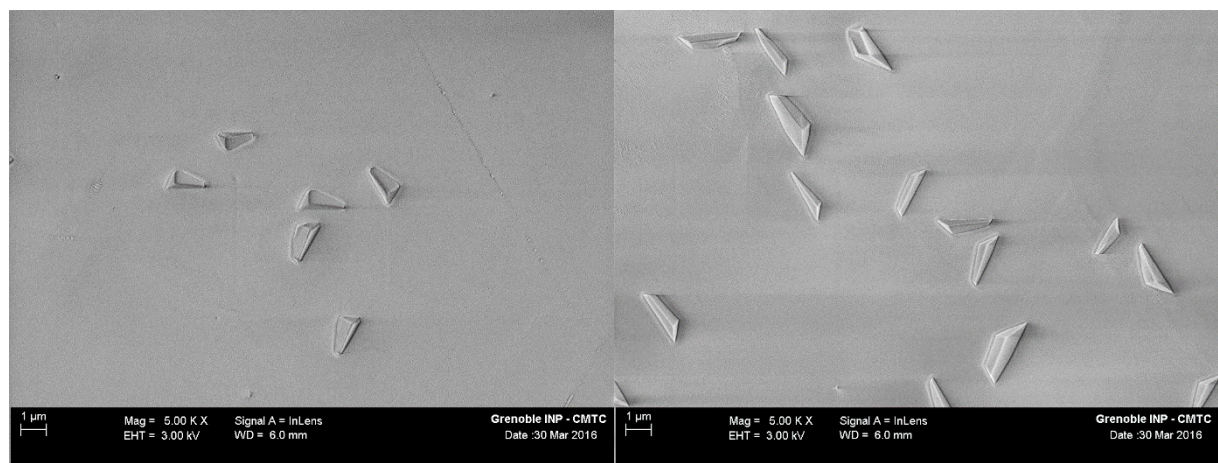


AIN-20





AIN-22



AIN-23

